J. Phys. B: At. Mol. Opt. Phys. 28 (1995) 309–339 Printed in the UK

TOPICAL REVIEW

Dynamics of H_2^+ in intense laser fields

A Giusti-Suzor†, F H Mies‡, L F DiMauro§, E Charron† and B Yang§

† Laboratoire de Photophysique Moléculaire, Bâtiment 213, Université Paris-Sud, 91405 Orsay, and Laboratoire de Chimie Physique, 11 rue Pierre et Marie Curie, 75231 Paris, France

‡ National Institute of Standards and Technology, Gaithersburg MD 20899, USA

§ Department of Chemistry, Brookhaven National Laboratory, Upton, NY 11973, USA

Abstract. A number of unexpected features of small molecules subjected to intense laser fields, with wavelengths ranging from infrared to ultraviolet, have been observed or predicted in the past few years: above-threshold dissociation, molecular bond softening, vibrational population trapping. We review these processes for the case of the molecular ion H_2^+ and discuss the experimental and theoretical tools that are used to study this system. Both electron and proton energy distributions are used to interpret the experimental results. Theoretically, the fragmentation dynamics can be described equivalently as a *laser-assisted half-collision* process, using solutions of the time-independent Floquet theory, or as the evolution of a *wavepacket* subjected to a classical radiation field with a given pulse shape, using solutions of the time-dependent Schrödinger equation. A broad range of laser intensity and pulsewidth has been explored, with the short-pulse results (analysed in terms of 'dressed' potential curves) offering the best interface between theory and experiment. We finally report on a promising new avenue for coherent control of fragmentation dynamics, through the use of two-colour phase-locked radiation.

1. Introduction

The production of ultra-short optical pulses has opened an exciting new chapter in the study of molecular dynamics. It is now a routine laboratory procedure to generate femtosecond laser pulses which are on the same time scale as the internal or external motion of molecules either in the gas or condensed phases. Recent experiments and theories in the strong-field limit ($> 10^{11}$ W cm^{-2}) have underscored the combined action of intramolecular couplings and molecule–field interactions in the time development of *half-collisions*, namely photodissociation and photoionization. This more exotic view of molecular processes has provided some fundamental insights into the fragmentation dynamics, as well as some useful analogies to strong-field atomic effects.

The attraction of such molecular studies derives from a fundamental interest in controlling chemical dynamics by variation of an external laser field. The traditional approach in photochemistry of using the laser frequency as the only external field parameter for achieving state-selective chemistry has met with limited success. However, recent efforts have focused on studying all aspects of the laser field for achieving control. Although premature in realization, understanding the influence of intensity, coherence, pulse duration, shaping and sequencing in concert with frequency may ultimately lead to our ability, or confirm our inability, to control chemical dynamics.

Experimental and theoretical studies have revealed a number of interesting features in strong-field photodissociation, which can only be understood in terms of complex multiphoton interactions, involving stimulated emission as well as absorption. From an energetic standpoint, these features are analogous to the more standard above-threshold

0953-4075/95/030309+31$19.50

ionization (ATI) picture (Agostini *et al* 1979, Gavrila 1992). In this picture a system (atom or molecule) can absorb *more* than the minimum number of photons necessary to free an electron or break a chemical bond. However, this bare energy balance offers little insight into the dissociation dynamics or potential distortion induced by the strong radiative couplings. A more intuitive feeling for this physics can be obtained by reformulating the problem in the framework of 'dressed' molecular states. We will show below that the dynamics is best analysed in this manner, although most of the calculations are now performed by direct numerical integration of the time-dependent Schrödinger equation. We stress that in the intensity range of these studies (10^{12}–10^{15} W cm^{-2}) perturbative treatments are inapplicable. We will see that the radiative field plays an active role not only in the excitation step, but also in the subsequent molecular dynamics which may be strongly influenced by radiative interactions among the final continuum states.

The pioneering experimental studies of molecules in strong laser fields were partly motivated by an interest to address, what was at that time, an outstanding issue in strong-field *atomic* physics, that is, whether multi-electron ionization proceeded via a *sequential* or a *direct* process. The physical distinction lies in whether the multiphoton production of highly charged ions proceeded via a sequence of one-electron ejections or by simultaneous removal of many electrons (direct process). Codling *et al* (1988) proposed examining the kinetic energy of photodissociation fragments of multicharged ions for evidence of a so-called 'Coulomb explosion'. In a direct process a large kinetic energy would be imparted to the ionic fragments by the Coulomb repulsion if the dissociative multielectron ionization happened abruptly at short interatomic distances through a 'vertical' multiphoton absorption. In contrast, a sequential mechanism, where the electrons are successively stripped from the molecule at larger distances as the ions separate would yield much lower kinetic energy in the atomic ions. This picture implicitly assumes that the individual photoionization processes, whether single or multielectron, occur rapidly compared to dissociation, such that the two events can be treated separately. Specific studies of the sequential *versus* direct processes in a variety of molecules, mostly diatomic (HI, I_2, N_2, CO, ...) but also polyatomic (alkanes), have recently been reviewed by Codling and Frasinski (1993). They show how the gross features of the experimental data can be discussed in terms of a simple classical field-ionization model. In general the sequential process has been observed to dominate the ionization dynamics.

In this review, we will concentrate on the strong-field behaviour associated with the simplest one-electron molecule, H_2^+, which is obviously a model system and has been the subject of extensive experimental and theoretical investigations. This molecule when irradiated by an intense laser field will either photodissociate,

$$H_2^+(1s\sigma_g, N_0, M_0, v_0) + n\hbar\omega \rightarrow H(1s) + H^+ \qquad (1a)$$

or ionize via a Coulomb explosion,

$$H_2^+(1s\sigma_g, N_0, M_0, v_0) + m\hbar\omega \rightarrow H^+ + H^+ + e^-. \qquad (1b)$$

Experimentally the details of both these mechanisms can be probed by use of energy-resolved mass and/or electron spectroscopy. The role of each process and their interplay will be discussed, with special emphasis on mechanism (1*a*) which dominates at moderate intensities, 10^{12}–10^{14} W cm^{-2}. The multiphoton ionization of H_2 will only be discussed within the context where the neutral molecule is used as the precursor in the formation of the molecular ion via the laser pulse. In actual fact, the ionization of H_2 has been well

established in some experiments (Normand *et al* 1986, Cornaggia *et al* 1986, Verschurr *et al* 1989, Bucksbaum *et al* 1990, Yang *et al* 1991) to proceed uncoupled from the subsequent H_2^+ photodissociation via

$$H_2(X^1\Sigma_g^+, J, M_J, v) + p\hbar\omega \rightarrow H_2^+(1s\sigma_g, N_0, M_0, v_0) + e^-. \tag{2}$$

Thus, for most cases it is reasonable to assume that the H_2 ionization occurs more rapidly than H_2^+ dissociation and, except for its importance for determining the initial distribution of internal states for paths (*1*) in the experiment, the two events from a theoretical standpoint can be treated separately. This point is essential if any detailed comparison is to be made between experiment and theory which assumes that the H_2^+ ion is prepared in a given stationary rovibrational level (N_0, M_0, v_0) of the ground $1s\sigma_g$ state. However, a recent experiment (Zavriyev *et al* 1993) using femtosecond pulse excitation raises some interesting questions concerning the simultaneous interplay between ionization and dissociation via the formation of a coherent vibrational wavepacket.

The photodissociation of H_2^+ in strong laser fields has been mostly described within the two-state model restricted to the attractive ground state $1s\sigma_g$ and the first repulsive $2p\sigma_u$ state, which both asymptotically dissociate to $H(1s) + H^+$ as in (*1a*) (we will discuss this limitation in section 2). This is shown schematically in figure 1 where the effect of absorbing $n = 1, 2, 3$ photons in reaction (*1a*) is portrayed. The final kinetic energy of the fragments ε_n is dependent on the net number of photons absorbed in the dissociation

$$\varepsilon_n \approx E(1s\sigma_g, N_0, M_0, v_0) + n\hbar\omega. \tag{3}$$

Understanding the dynamics of the dissociation, and predicting the fragment energy distribution will be the major subject of this review.

A preview of the various effects that will be discussed is best obtained by examining the curves in figure 2, which represent the field-dressed version of the potential curves in figure 1. For a given electronic state φ_i and a given photon number $|N - n\rangle$ which is meant to describe a laser field with n photons removed by absorption, we construct the *diabatic* field-dressed state $\varphi_i|N - n\rangle$ with total energy $V_i(R) + (N - n)\hbar\omega$. For example, the initial electronic–radiative state in equation (*1a*) is represented as $\varphi_g|N\rangle$ with a total energy $V_g(R) + N\hbar\omega$. This energy has been scaled to zero at $R = \infty$ and denotes the $g, n = 0$ limit in figure 2. Absorption of an odd number of photons, such as $n = 1$ or $n = 3$ in figure 1, leads to a final electronic–radiative state $\varphi_u|N - n\rangle$ with a total energy $V_u(R) + (N - n)\hbar\omega$, corresponding to the displaced $u, n = 1$ or $u, n = 3$ curves in figure 2. Absorption of an even number of photons leads back to the initial $1s\sigma_g$ state with n photons removed and the total energy for the $g, n = 2$ channel in figure 2 is displaced accordingly.

Generally, as the intensity increases, the diabatic curves themselves are not sufficient to understand the dynamics, and much better physical insight is obtained from the broken curves in figure 2 which represent the so-called adiabatic field-dressed potentials (Kroll and Watson 1976, Lau 1977, Yuan and George 1978, Bandrauk and Sink 1978, 1981) obtained by diagonalizing the molecule-field Hamiltonian at fixed internuclear distance R. In the dipole approximation only radiative number states which differ by ± 1 photon are directly coupled, and thus, for a given pair of diabatic curves with n and $n + \Delta$ photons removed from the radiation field, the magnitude of Δ gives the expected order of their radiative interaction. The degree of adiabaticity is dependent on the intensity of the field, and on Δ.

The next section of the paper will introduce the theoretical framework necessary to describe strong-field photodissociation processes including both time-independent and

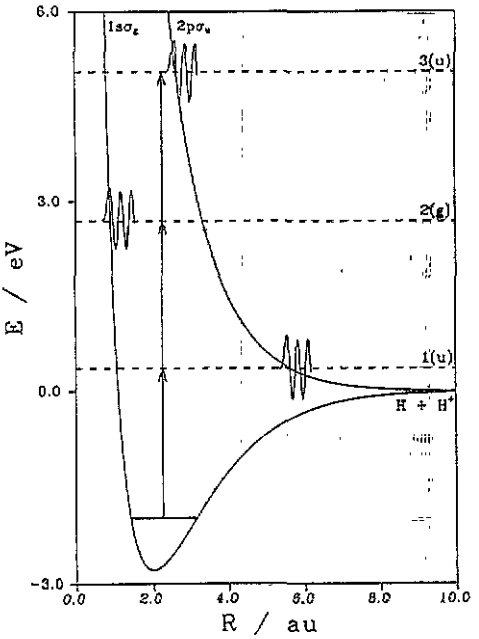

Figure 1. Potential energy curves for the $1s\sigma_g$ and $2p\sigma_u$ states of H_2^+, showing schematic continuum nuclear wavefunctions after absorption of 1, 2 or 3 photons of wavelength 532 nm, from the $v_0 = 2$ level in the ground state.

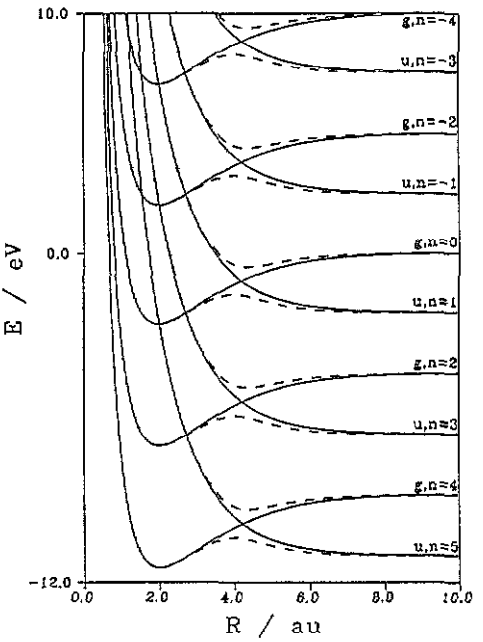

Figure 2. Potential energy curves for the $1s\sigma_g$ and $2p\sigma_u$ states of H_2^+, dressed with ± 5 photons of wavelength 532 nm. The full curves correspond to 10 interacting 'diabatic' channels. The dotted curves represent the field-dressed 'adiabatic' potentials obtained by diagonalizing the length-gauge radiative interaction for $I = 1.5 \times 10^{13}$ W cm^{-2}, using a basis set of 60 diabatic states.

time-dependent methods. A brief description of a typical experimental apparatus and the multiphoton ionization processes leading to the molecular ion will be addressed in the third section. Section 4 will review the various fragmentation processes observed or predicted, analyse them within the 'dressed' state picture, and compare experimental and theoretical results whenever both are available. The final section will conclude with some speculation for future directions.

2. Theoretical methods

All the calculations that have been performed on the photodissociation of H_2^+ in strong fields only include radiative coupling between the attractive ground state $1s\sigma_g$ and the first repulsive $2p\sigma_u$ state, both of which asymptotically dissociate to H(1s) + H^+ as in equation (1*a*) and figure 1. Explicitly the electron–nuclear wavefunction for the H_2^+ molecular ion, which should contain a complete set of electronic states, is restricted to the two electronic wavefunctions $\varphi_g(r, R)$ and $\varphi_u(r, R)$ associated with these states:

$$\Phi(r, R, t) = \varphi_g F_g(R, t) + \varphi_u F_u(R, t). \tag{4}$$

Especially notable is the absence of ionization continuum states which would be needed to simulate the competition between ionization and dissociation, a process that should become

important at very large field intensities. We will briefly consider this limitation in section 2.5. In the various calculations that have been presented in the literature the radiative interaction between the two electronic states in equation (4) has been represented either in the electric field gauge (length form) or in the Coulomb gauge (velocity form). In both cases the radiative coupling is induced by the electronic transition dipole $\mu_{gu}(R) = \langle\varphi_g|(ez)|\varphi_u\rangle$ and proportional to the electric field of the linearly polarized laser

$$\boldsymbol{E}(t) = f(t)E_{max}\cos(\omega t)\hat{\boldsymbol{e}} = E(t)\hat{\boldsymbol{e}} \tag{5}$$

with frequency ω and maximum field amplitude E_{max}. The time-dependent envelope $f(t)$ defines the pulse shape of the laser, and $\hat{\boldsymbol{e}}$ is the polarization vector.

For the moment we will make the other prevailing assumption that the H_2^+ molecule is perfectly aligned in the direction of $\hat{\boldsymbol{e}}$. This field-aligned approximation, which we refer to as the 1D model, decreases the required computational time by an order of magnitude or more, and yet appears to give an excellent representation of the dynamics. It is discussed in detail in section 2.4, and calculations will be presented which confirm its validity for strong fields. Assuming that the internuclear coordinate $\boldsymbol{R}$ is oriented along $\hat{\boldsymbol{e}}$, the radiative coupling in the length gauge is

$$\hbar\Omega_{gu}(R,t) = \langle\varphi_g|\boldsymbol{E}(t)\cdot(e\boldsymbol{r})|\varphi_u\rangle = E(t)\mu_{gu}(R). \tag{6}$$

Because of the asymptotic degeneracy of the two electronic states the transition dipole increases monotonically at large R, $\mu_{gu} \to eR/2$ (see e.g. Bates 1951), and Ω_{gu} actually diverges as $R \to \infty$. In contrast, the radiative coupling in the Coulomb or velocity gauge,

$$\hbar\Omega_{gu}^{vel}(R,t) = \langle\varphi_g|\boldsymbol{p}\cdot\frac{e}{c}\boldsymbol{A} + \left(\frac{e}{c}\boldsymbol{A}\right)^2|\varphi_u\rangle = \frac{(V_g - V_u)}{\hbar\omega}\hbar\Omega_{gu}(R,t) \tag{7}$$

where $\boldsymbol{A}$ is the potential vector associated with $\boldsymbol{E}$, vanishes asymptotically since the splitting between the molecular potentials decreases exponentially as $R \to \infty$. Thus, it is tempting to use this gauge, especially in time-independent or Floquet-type calculations, in order to avoid troublesome asymptotic boundary conditions.

Obviously if a complete basis of electronic states were employed in the calculations the dynamics would, of necessity, be gauge invariant. However, depending on the gauge the two-state model can give order of magnitude differences for multiphoton processes, and it is not evident *a priori* whether either of these representations of the radiative coupling give a good representation of the actual dissociation dynamics. In section 2.1 we present the evidence, based primarily on some field-dressed variational calculations by Muller (1992), that the two-state approximation for H_2^+ is very well justified, but only using a length gauge radiative coupling.

Two complementary methods are commonly used for solving this two-state field-aligned model. The time-independent Floquet-type theory, which was the first method applied to H_2^+, is discussed in section 2.2. This technique is especially good for moderately intense, long-time laser pulses, although the requirement of introducing the asymptotically divergent length-gauge coupling has dampened enthusiasm for this approach. The currently most used method, especially for short intense laser pulses, is to numerically solve the time-dependent Schrödinger equation, and this is discussed in section 2.3. The validity of the 1D model is confirmed by comparison with exact 3D results in section 2.4. Finally we discuss the competing effect of photoionization in section 2.5 and present some characteristic photoionization rates that have been calculated for H_2^+.

Those readers who are more concerned with the experimental techniques and discussion of the fragmentation dynamics may wish to proceed to section 3.

2.1. Confirmation of two-state, length-gauge model of H_2^+

The time-dependent Schrödinger equation in the interaction picture for H_2^+, using the Coulomb (velocity) gauge, is

$$\left[\frac{1}{2\mu}p_R^2 + \frac{1}{2m_e}\left(p + \frac{e}{c}A\right)^2 + V_{coul}\right](e^{-i\Lambda}\Psi) = i\hbar\frac{\partial}{\partial t}(e^{-i\Lambda}\Psi) \tag{8}$$

where μ is the reduced nuclear mass. Using the following gauge transformation

$$\Lambda(t) = \frac{e}{c\hbar}A(t)\cdot r \qquad \hbar\frac{\partial\Lambda}{\partial t} = E(t)\cdot(er) \tag{9}$$

where r is the electronic coordinate conjugate to p, we obtain the usual time-dependent Schrödinger equation in the length gauge,

$$\left[\frac{1}{2\mu}p_R^2 + H_0 + E(t)\cdot(er)\right](\Psi) = i\hbar\frac{\partial}{\partial t}(\Psi). \tag{10}$$

The field-free electronic Hamiltonian

$$H_0 = \frac{1}{2m_e}p^2 + V_{coul}$$

for H_2^+ generates a complete set of molecular electronic states $\{\varphi_i\}$ and associated molecular potentials $\{V_i(R)\}$ which span the space of r at each internuclear distance R. This set includes the two lowest states φ_g and φ_u used in the expansion (4).

Two choices have been made in treating the photodissociation problem: one is to use the wavefunction Φ given by equation (4) in place of $e^{-i\Lambda}\Psi$ in equation (8) and solve the two-state model in the Coulomb gauge; the second is to use Φ to approximate Ψ in equation (10) and instead solve the two-state model with length-gauge coupling. It should be noted from equation (7) that the two gauges give the same coupling strength in the vicinity of a one-photon 'resonance' where the classical Franck–Condon principle requires $(V_g - V_u) \approx \hbar\omega$. In contrast a process involving Δ photons can be expected to occur primarily around the distance where $(V_g - V_u) \approx \Delta\hbar\omega$ and the couplings predicted by equations (6) and (7) differ by factors of Δ. Thus, it is not surprising that the predicted dynamics differ strongly.

Aside from the currently intractable task of solving (8) or (10) exactly, an attractive alternative would be to expand equation (4) in a set of field-dressed electronic states. This could be generated by numerically solving the electronic portion of equation (8) or (10) for a set of time-dependent electronic states $\{\Omega_k(t)\}$ with the nuclear kinetic energy operator $(1/2\mu)p_R^2$ removed. An excellent criterion on the numerical accuracy of such a project would be to obtain identical solutions $\{\Omega_k(t)\}$ using either gauge

$$\left[\frac{1}{2m_e}\left(p + \frac{e}{c}A\right)^2 + V_{coul}\right](e^{-i\Lambda}\Omega) = i\hbar\frac{\partial}{\partial t}(e^{-i\Lambda}\Omega) \tag{11a}$$

or

$$[H_0 + E(t)\cdot(er)](\Omega) = i\hbar\frac{\partial}{\partial t}(\Omega). \tag{11b}$$

This gauge-invariant criterion is well satisfied in the variational calculations of Muller (1992) using Floquet theory to solve equation (11), and in the time-dependent results of Mies *et al* (1993). The Floquet results of Muller were obtained by performing a Fourier expansion of the field-dressed states in equation (11):

$$\Omega_k(t) = \sum_n \Omega_{n,k} \exp(-in\omega t) \exp\{-iV_k(R)t\} \tag{12}$$

and expanding the Fourier components $\Omega_{n,k}$ in an electronic basis sufficient to obtain a converged set of gauge-invariant solutions to both equations (11*a*) and (11*b*). The resultant R-dependent eigenvalues $V_k(R)$ depend on the maximum field strength E_{max} and define a set of adiabatic field-dressed molecular potentials. The potentials for $\lambda = 532$ nm are shown in figure 3, for two different field intensities. The exact adiabatic field-dressed potentials obtained using a complete variational solution for Ω_k (Muller 1992) are compared to the results obtained just using the two lowest field-free states to expand $\Omega_{n,k}$ in equation (12), for fixed R ranging from 1 to 6 au. It is quite clear that the two-state approximation to the length-gauge expression (11*b*) gives almost perfect agreement with Muller, while the two-state solution to the velocity-gauge expression (11*a*) yields unacceptable results.

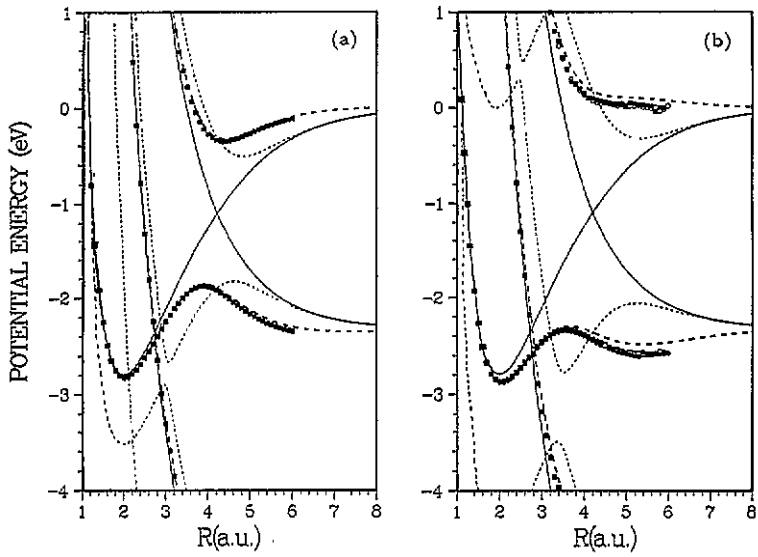

Figure 3. Same as figure 2 for (a) $I = 3.16 \times 10^{13}$ W cm^{-2} (b) $I = 8.78 \times 10^{13}$ W cm^{-2}, in the region of the $n = 0$ and $n = 1$ curve crossing. The adiabatic curves obtained within the two electronic state model with radiative interaction expressed in the length gauge (broken) or the velocity gauge (dots) must be compared to the exact gauge invariant results of Muller (1992) shown in both the length (circles) and the velocity (squares) gauges.

Although somewhat indirect, substantial evidence for the validity of the two-state model in the length-gauge representation is also inferred from an analysis of the photoionization rates for H_2^+ obtained by numerical solution of the time-dependent Schrödinger equation (11*b*) at fixed R (see section 2.5). The exact ionization rates could be modelled quite accurately by a simple length-gauge coupling of the two electronic states φ_g and φ_u in equation (4) combined with optical potentials to represent the ionization of

the resultant pair of field-dressed electronic states. The model was found to give good results for a wide range of wavelengths and intensities. At very short wavelengths (e.g. 228 nm) states other than the two lowest ones appear to contribute to ionization (Chelkowski *et al* 1992, Mies *et al* 1993) and any two-state dissociation calculations must be viewed with reservation even if the length gauge is employed. Fortunately, for the wavelengths $\lambda = 1064, 780, 532, 340, 322$ nm used in the experiments, the two-state length-gauge model gives reliable results.

2.2. *Long-time pulses: use of time-independent Floquet theory*

The non-perturbative time-independent theory of strong-field photodissociation can be derived in two ways, depending on whether the radiation theory is treated classically or quantally, leading to practically identical formulations. In both cases it is assumed that the electric field in equation (5) is turned on abruptly at $t = 0$ with $f(t) = 1$ and a prescribed maximum intensity E_{max} is maintained indefinitely. Since the theories implicitly involve averaging the radiative coupling over an optical cycle, this is a good model for a long, moderately intense laser field where the dynamics is very slowly varying over a few optical cycles and insensitive to any transient behaviour introduced by the abrupt turn-on.

One can start from a classical representation of the laser oscillating electric field and perform a Fourier expansion of the radiative interaction and of the resulting molecular wavefunctions (Floquet theory, see e.g. Shirley 1965, Chu 1981). This is analogous to what was done in equation (12) to obtain the adiabatic field-dressed potentials. Alternatively (Kroll and Watson 1976, Lau 1977) one can use the quantal formulation of the radiative field with creation and annihilation operators associated with photon emission and absorption. In this case, one defines a set of photon number states $|N-n\rangle$ centred around a large N photon number proportional to the field intensity and solves a set of coupled scattering equations for a prescribed total energy E:

$$\Psi(r, R, N, E) = \sum_{n=\text{even}} |N-n\rangle\varphi_g F_{n,g}(R, E) + \sum_{n=\text{odd}} |N-n\rangle\varphi_u F_{n,u}(R, E). \tag{13}$$

The molecule-field channel state $|N-n\rangle\varphi_g$ with $n = 0$ defines the initial state of the system before any absorption ($n > 0$) or stimulated emission ($n < 0$) has occurred. The index n is related to the usual 'Floquet number' n in equation (12) which becomes identified with photon absorptions and emissions in the classical theory. The advantage of this quantum number state approach is that it allows one to construct realistic wavepackets to describe half-collision events, such as photodissociation and photoionization, which can involve complicated non-exponential decay of the target in intense fields (see Mies and Giusti-Suzor 1991). Starting from a set of dressed channels in equation (13) coupled by time-independent radiative couplings, any of the numerical techniques used in close-coupling scattering theory can be applied for solving the corresponding system of coupled equations: complex scaling of the R-coordinate (Chu 1981, 1991, He *et al* 1988, 1990), Fox–Goodwin propagation with adjunction of an artificial channel (Bandrauk and Sink 1981, Bandrauk *et al* 1993), renormalized Numerov (Giusti-Suzor *et al* 1990). The initial vibrational level is viewed as a resonant state in a specific closed channel, with its laser broadening (proportional to the dissociation rate) and AC–Stark shift easily extracted from the numerical results. The methods based on a full-collision formalism (Mies and Giusti-Suzor 1991) with outgoing waves in each open dressed channel easily yield the branching ratios for dissociation with varying amounts of absorbed photons. These quantities are the most clear signature of the dynamical events induced by the strong radiative field in the dressed molecule, and are directly related to the photofragment energy spectra recorded in the experiments.

As demonstrated in section 2.1 the asymptotically convergent velocity-gauge coupling is invalid. On the other hand, the asymptotic divergence of the transition moment as $R/2$ in the length form complicates the time-independent scattering formulation of the fragmentation process where the laser intensity is assumed to stay constant out to infinite distances. Remedies have been proposed to overcome this difficulty (see e.g. Chrysos *et al* 1993) but fortunately this problem is avoided for short laser pulses treated in a time-dependent approach since then the radiative interaction vanishes well before the particles reach large internuclear distances.

2.3. Short-time pulses: use of wavepacket and time-dependent theory

For laser pulses in the subpicosecond domain, the field intensity varies on the time scale of the fragmentation process and the pulse shape has to be explicitly included in the calculations. Thus, time-dependent treatments have been adopted by most theoretical groups in the last two years, especially in view of the increased use of short-pulse lasers.

A molecule in the initial stable state v_0 is subjected to a Gaussian laser pulse of width T_p, corresponding to the classical electrical field $\boldsymbol{E}$ linearly polarized along $\hat{e}$ as given in equation (5). The pulse shape is often approximated by the Gaussian-like expression $f(t) = \sin^2(\pi t/2T_p)$ with total pulse duration $2T_p$, to avoid the extended wings of the true Gaussian shape which lengthen the calculations without any noticeable contribution to the physical processes. The time-dependent Schrödinger equation is directly solved by any of the available methods for wavepacket propagation with time. The most commonly used in this domain is the splitting technique of the short-time propagator (Feit *et al* 1982, Heather 1991), which transforms the wavefunction back and forth between the coordinate (R) and the momentum (k) representations, using fast Fourier transformations (FFT). In addition, Heather (1991) introduced an asymptotic splitting algorithm which separates the wavepacket into coupled and uncoupled portions at some internuclear distance R_s beyond the interaction region. This allowed substantial economy in computer times when calculations were performed using the convergent velocity-gauge coupling, with a typical $R_s \approx 25$ au (Heather and Mies 1991). Use of such numerical techniques in the length gauge requires additional transformations at long range (Kellar 1994).

These time-dependent calculations provide the temporal evolution of the molecular wavepacket, in particular the decay of the initial bound-state population and the dissociation probability at the end of the laser pulse. The probability of observing $H(1s)+H^+$ fragments with asymptotic relative kinetic energy ε,

$$P(\varepsilon) = |C_g(\varepsilon)|^2 + |C_u(\varepsilon)|^2 \tag{14}$$

is obtained by numerically evaluating the projections $C_g(\varepsilon) = \langle g, \varepsilon | F_g \rangle$ and $C_u(\varepsilon) = \langle u, \varepsilon | F_u \rangle$ of the wavepacket at the conclusion of the pulse ($t = 2T_p$) onto the two complete sets of outgoing continuum wavefunctions $|g, \varepsilon\rangle$ and $|u, \varepsilon\rangle$ in the uncoupled molecular potentials V_g and V_u respectively. All subsequent dynamics of the field-free wavepacket is completely determined by these coefficients, their magnitude remaining independent of time. Aside from the computational virtues of using this projection rather than numerically following the field-free wavepacket to long times, we have found this method imperative for obtaining reliable estimates of $P(\varepsilon)$ if very slow photofragments contribute to the dissociation.

2.4. Three-dimensional calculations and confirmation of field-aligned model

Most previous calculations have been performed using the field-aligned (or 1D) model, where $\boldsymbol{R}$ in the radial functions F_g and F_u of equation (4) is constrained to be perfectly aligned along the polarization axis of the laser field. Initially this was based on experimental evidence (Normand *et al* 1992, Strickland *et al* 1992) and presumably results from rapid multiphoton 'optical pumping' to rotational states (N, M) with high angular momentum N and low spatial projections. More recently the time-dependent theory has been extended (McCann and Bandrauk 1992, Aubanel *et al* 1993a, b, Charron *et al* 1994a) to treat the full 3D problem.

The radial functions in equation (4) are expanded in a large but finite set of spherical harmonics, $Y_{N,M_0}(\theta_R, \phi_R)$ which define the angular momentum and span the angular coordinates associated with $\boldsymbol{R} = (R, \theta_R, \phi_R)$:

$$F_{g(u)}(\boldsymbol{R}, t) = \sum_N Y_{N,M_0}(\theta_R, \phi_R) F_{N,M_0}(R, t). \tag{15}$$

The target $H_2^+(1s\sigma_g)$ molecule in equation (1*a*) can now be completely specified to be in the v_0 vibrational state with nuclear angular momentum N_0 and space-fixed projection M_0 (the space-fixed axis is chosen to coincide with the polarization axis of the laser and therefore $\boldsymbol{R} \cdot \hat{\boldsymbol{\epsilon}} = Z \equiv R\cos\theta_R$). Since the laser field is linearly polarized the initial azimuthal quantum number M_0 is always conserved in equation (15).

In analogy to the procedures used to obtain $P(\varepsilon)$ for the 1D model in equation (14), the analysis of the angular distribution can be made using the energy normalized solutions of the field-free dissociated molecular states. The procedure is well described in a series of articles by Singer *et al* (1983, 1984) and specifically applied to H_2^+ by Charron *et al* (1994a). Basically we need to define the set of 'outgoing' plane waves elastically scattered by both uncoupled g and u states in the direction of the interatomic wavevector $\boldsymbol{k} = k\hat{\boldsymbol{k}} = (k, \theta_k, \phi_k)$, for a prescribed asymptotic relative kinetic energy $\varepsilon = \hbar^2 k^2/2\mu$. These are represented by the usual expansion in nuclear angular momentum states, or partial waves, N. For example, the ungerade state yields,

$$|\mathrm{u}, \varepsilon, \hat{\boldsymbol{k}}\rangle = \sum_N Y_{N,M_0}(\theta_k, \phi_k) \mathrm{i}^N \mathrm{e}^{-\mathrm{i}\xi(\mathrm{u},N)} |\mathrm{u}, \varepsilon, N, M_0\rangle \tag{16a}$$

where $Y_{N,M_0}(\theta_k, \phi_k)$ are the spherical harmonics associated with the wavevector $\boldsymbol{k}$, and

$$|\mathrm{u}, \varepsilon, N, M_0\rangle \rightarrow \varphi_u Y_{N,M_0}(\theta_R, \phi_R) \left(\frac{2\mu}{\hbar^2 \pi k}\right)^{1/2} \sin(kR - \pi N/2 + \xi)/R \tag{16b}$$

represents the energy-normalized continuum state for the Nth partial wave scattered by the field-free potential $V_u(R)$ yielding the scattering phaseshift $\xi(\mathrm{u}, N)$. A similar outgoing expression is obtained for the gerade state. At the conclusion of the pulse the amplitudes

$$C_u(\varepsilon, \hat{\boldsymbol{k}}) = \mathrm{e}^{\mathrm{i}\varepsilon 2T_p/\hbar} \langle \mathrm{u}, \varepsilon, \hat{\boldsymbol{k}} | \varphi_u F_u(\boldsymbol{R}, 2T_p)\rangle \tag{17}$$

are evaluated, with comparable gerade amplitudes $C_g(\varepsilon, \hat{\boldsymbol{k}})$ projected from $F_g(\boldsymbol{R}, 2T_p)$. Again, all subsequent dynamics of the field-free wavepacket is completely determined by these coefficients whose magnitude remains independent of time. The probability for a

bare proton to escape in the $\hat{k} = (\theta_k, \phi_k)$ direction and a neutral H(1s) in the opposite $-\hat{k} = (\pi - \theta_k, \pi + \phi_k)$ direction is related to these projections (Charron *et al* 1994a):

$$P_{H^+}(\varepsilon, \hat{k}) = P_{H(1s)}(\varepsilon, -\hat{k}) = \tfrac{1}{2}|C_g(\varepsilon, \hat{k}) - C_u(\varepsilon, \hat{k})|^2. \tag{18}$$

The calculated proton angular distributions shown in figure 4 originate from an initial rovibrational level ($v_0 = 3, N_0 = 0, M_0 = 0$) subjected to a 780 nm radiation with a peak intensity of 10^{14} W cm^{-2} and a pulse width $T_p = 150$ fs. The plot in the inset gives visual confirmation that the proton angular distribution mainly consists of two symmetric peaks centred around 0° (forwards ions) and 180° (backwards ions). Analysis of the wavepacket at the end of the pulse indicates that a distribution of partial wave components $Y_{N,0}$ ranging from $N = 0$ to 16 coherently yields the distributions in figure 4. As expected for a single-colour laser there is perfect symmetry of the proton distribution in the forward and reverse directions of the laser polarization. It can be shown that the symmetry $P_{H^+}(\varepsilon, \hat{k}) \equiv P_{H^+}(\varepsilon, -\hat{k})$ is only broken if both the gerade and ungerade states contribute to the *same kinetic energy* in equation (18). This may happen with phase-locked two-colour ($\omega + 2\omega$) lasers whenever the second harmonic frequency is used, as we shall see in section 4.3.

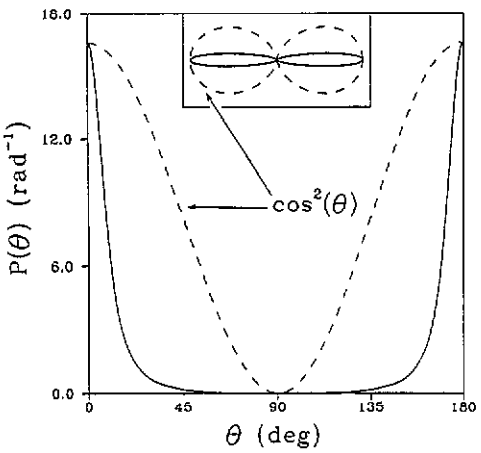

Figure 4. Proton angular distribution (full curve) in the dissociation of the initial ($v_0 = 3, N_0 = 0, M_0 = 0$) level of H_2^+ ground state with a 780 nm, $I = 10^{14}$ W cm^{-2} laser pulse of half-duration 150 fs. The inset represents the contour of the angular distribution with respect to the laser polarization axis ($\theta = 0$), compared with a $\cos^2\theta$ distribution (broken curve) corresponding to a one-photon Σ–Σ transition. The total dissociation probability is 93.6% and the largest rotational components for the dissociating portion of the wavepacket correspond to $N = 2, 4, 6$.

More explicit evidence of the multiphoton optical pumping origin of this alignment phenomenon is seen in figure 5, which shows the spatial distribution of the wavepacket for an initial ($v_0 = 3, N_0 = 0, M_0 = 0$) molecule which produced the proton spectrum in figure 4. Before the pulse the distribution is perfectly isotropic in space, and exhibits the three nodes associated with a $v = 3$ state. At the peak ($t = T_p$) the molecule is reasonably aligned along the polarization axis of the field. (Note that a big 'piece' of the wavepacket is located in the vicinity of $X = \pm 4$ au. The significance of this 'population trapping effect' will be discussed in detail in section 4.2.) At the conclusion of the pulse we are left with 6.4% of aligned molecules, mostly in a $v = 1$ state, combined with some $v = 2$ and 3. This vibrational packet also consists of a coherent superposition of rotational states $Y_{N,0}$ with a range of $N \approx 4$–12. It is interesting to note that the largest component (2.3%) in the wavepacket, ($v = 1, N = 12$) has an energy very close to the initial internal energy $E_g(v_0 = 3, N_0 = 0)$ of the molecule, and the alignment of the ion by optical pumping seems to favour 'on the energy shell' transitions. This effect helps explain why there is less

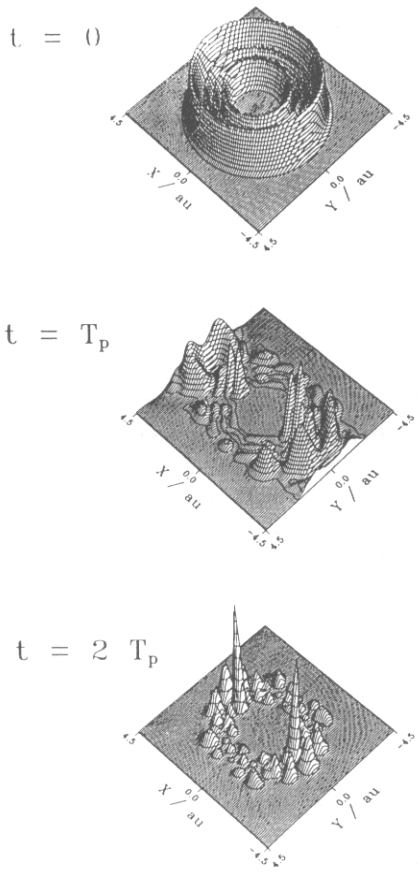

Figure 5. Two-dimensional representation (with the laser polarization along the x-axis) of the same wavepacket as in figure 4, before, at the middle and at the end of the pulse of half-duration $T_p = 150$ fs. The bound population at the end of the pulse ($t = 2T_p$) is predominantly in the $v = 1, N = 12, M = 0$ rovibrational level, to be compared with the initial $v_0 = 3$, $N_0 = 0$, $M_0 = 0$ level.

apparent broadening in the asymptotic kinetic energy distributions than might be surmised from the increase in the mean value of N.

These results give us a good deal of confidence that the semiquantitative features predicted by the 1D models are close to reality. In section 4.2 we will return to this problem and discuss the influence of rotation on the stabilization of H_2^+ in intense fields.

2.5. *Competition with ionization of H_2^+ in strong field and Coulomb explosion*

Although the complete time-dependent Schrödinger equations (8) or (10) for the simultaneous ionization and dissociation of H_2^+ in an intense laser field cannot easily be solved, current technology allows one to solve equation (11) and calculate the probability of ionization of a perfectly aligned molecule at a fixed bond-length R. A strong motivation for such calculations is to test the reliability of neglecting ionization in the simple two-state model of dissociation. This is especially urgent, since, as we shall see in section 4, in intense short-pulse laser fields an appreciable population can survive beyond the peak of the pulse. This survival effect can be attributed to the trapping of portions of the vibrational wavepacket in transient laser-induced potential wells at intermediate distances (R = 3–6 au). Having accurate R-dependent ionization rates enables us to estimate the competitive influence of the ionization on the stabilized population, and may ultimately allow us to predict the contribution of the 'Coulomb explosion' channel to observed proton kinetic energy distributions, as will be discussed in section 4.2.

The first such calculation of ionization rates was done by Chelkowski *et al* (1992) for an intense $\lambda = 228$ nm laser and the results indeed show a strong dependence of the rate constant on the internuclear distance R. Comparable time-dependent calculations for H_2^+ in fields of $I \leqslant 10^{15}$ W cm^{-2} for a wide range of R (2–8 au) and wavelengths (228–1064 nm) have been done by Mies *et al* (1993) and indeed this same effect persists. As expected, at large R the ionization rate for all wavelengths rapidly approaches that of H(1s).

In order to properly discuss the experimental results obtained with the 150 fs, $\lambda = 769$ nm Ti:sapphire laser which have been interpreted as exhibiting Coulomb explosion (Zavriyev *et al* 1993), it will be useful to have these specific ionization probabilities available. They are presented in figure 6 for three different field intensities as a function of R, after 20 optical cycles (51 fs). Note that near the equilibrium distance $R \approx 2$ au the large ionization potential (29 eV) of the molecule allows it to easily survive intensities in the 10^{14} W cm^{-2} range, for typical pulses of 150 fs.

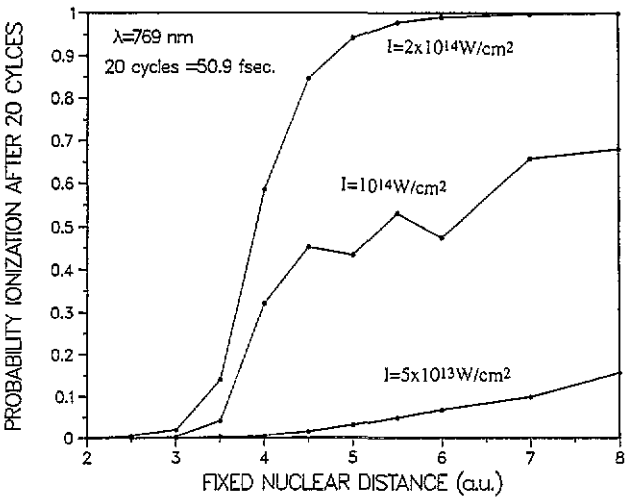

Figure 6. Ionization probability of the H_2^+ ion for several internuclear distances R, after 20 optical cycles of a 769 nm radiation at three different intensities.

As mentioned previously, the ionization rates obtained from the exact numerical solution of the time-dependent Schrödinger equation have been found (Mies *et al* 1993) to conform beautifully with a very simple representation of H_2^+ which only involves its two lowest electronic states $1s\sigma_g$ and $2p\sigma_u$ coupled in the length gauge, and an optical potential to represent the ionization. This simple model works very well for $\lambda = 769$ nm and will be useful for estimating the relative contribution of the Coulomb explosion to the photodissociation process.

It is interesting to note that Chelkowski *et al* (1993) also calculated the harmonic generation spectrum for H_2^+ at fixed internuclear distance and found a substantial enhancement of the cross sections associated with the asymptotic resonant charge exchange contribution to the transition dipole.

3. Experimental details

3.1. Apparatus

The specific experimental details will be discussed in the appropriate subsections, here we just review the basic features. Furthermore, we are only considering the experimental concerns necessary for studying strong-field dissociation of H_2^+, which fragments along the polarization axis. An experimental apparatus will usually consist of a well-characterized laser system capable of producing intensities in the range of 10^{14-16} W cm^{-2} which is focused into an ultra-high vacuum system equipped with energy-resolved ion mass and/or photoelectron spectrometers. Time-of-flight spectrometers are typically employed with variations in designs for spatial collection efficiency. A typical energy resolution for an electron and ion mass spectrometer is 5% and 10%, respectively. In order to acquire energy resolution from the ion mass spectrometer a small uniform DC field is placed across the interaction volume parallel to the detection axis of the spectrometer. When the laser polarization is fixed parallel to this field, the dissociation fragments (protons) have two distinct arrival times at the detector which correspond to fragments with initial velocities moving towards or away from the detector. The kinetic energy of the fragments is simply determined by measuring the arrival time difference between the two peaks. Photoelectron spectroscopy is an effective diagnostic tool for determining the H_2^+ initial distribution, as will be discussed below, as well as a probe of the ionization dynamics of the molecular ion.

Care must be taken in minimizing space-charge effects in any strong-field measurement which produces ions. The interaction volume, defined by the laser spot size, will ultimately determine the amount of charge that can be produced within the focus, that is, the maximum tolerable target density. This effect is immediately evident in an experiment by a degradation in collection efficiency, energy, and angular resolution of a spectrometer. Typical spot sizes of 3–10 μm beam radius limit the ion yield to approximately 50–100 ions/laser shot. Another major issue which will be discussed in the next section is the preparation of the hydrogen molecular ion.

3.2. Ion preparation

For any detailed interpretation of an experiment a working knowledge of the target species initial conditions is crucial. This point is further amplified in molecular studies compared to atomic due to the complexity of the additional degrees of internal motion. For studies which involve transient species, such as the hydrogen molecular ion, sample preparation becomes an experimental necessity which can be achieved in a variety of ways, e.g. by electron impacts, laser excitation, each of which can produce varying degrees of selectivity. To date, all strong-field dissociation studies, including hydrogen, have relied on laser excitation. Unfortunately, for strong-field photodissociation studies of H_2^+, the laser pulse which initiates the fragmentation is the same pulse which produces the target molecular ion via multiphoton ionization of the neutral precursor. This has consequences for producing a *non-selective* and, most importantly, an *intensity-dependent* initial-state distribution. In this section we will examine the issue of multiphoton ionization of the hydrogen molecule as it pertains to interpreting the dissociation data of the molecular ion.

For the most part, multiphoton ionization of molecules has been used as a spectroscopic probe of the structure and dynamics of molecular systems. However, some groups have examined the influence of a strong field in altering the molecular structure or ionization dynamics. One can immediately expect all the effects, i.e. above-threshold ionization (ATI), channel closure, found in strong-field atomic ionization (Freeman *et al* 1988, Freeman and

Bucksbaum 1991). The anticipated complications expected from the additional degrees of freedom turn out in practice to be quite tractable, although experimentally more demanding.

The strong-field dissociation investigations have used photoelectron spectroscopy as the main diagnostic in determining the H_2^+ initial-state distribution. Due to the limited energy resolution of the photoelectron spectrometers discussed above, rotational structure is unresolvable but vibrational content is easily discernible, especially for light diatomics. The type of information which can be extracted from the photoelectron spectrum depends strongly on the time domain of the experiment (Helm *et al* 1991, Gibson *et al* 1991). In the long-pulse limit (pulse duration $T_p > 1$ ps) where the electron gains ponderomotive energy as it leaves the beam waist adiabatically, the ion final-state vibrational information is preserved. However, for shorter pulses ($T_p < 1$ ps) the intermediate electronic states are directly observable due to Stark shifting resonances, analogous to the atomic case. The unfortunate consequence, though, is the loss of information about the final-state vibrational content when, as is often the case, Rydberg intermediate resonances dominate the ionization dynamics. This results from the Stark shift of the Rydberg intermediate states being approximately equivalent to the threshold ponderomotive shift, a first-order cancellation of the vibrational frequency between the Rydberg intermediate state and the ionic ground state, and the $\Delta v = 0$ propensity rule. The study of Helm *et al* (1991) clearly demonstrates a dramatic simplification of the hydrogen molecule photoelectron spectrum resulting from 100 fs, UV multiphoton ionization. The spectrum consists of a number of peaks corresponding to a Rydberg series with different principal quantum numbers. However, a modest change in the UV frequency excites the H_2 valence B state resulting in a more complex spectrum which manifests the ion vibrational content. Similar observations have been seen in other diatomic molecules (Gibson *et al* 1991).

We will begin by examining the long-pulse, green excitation of the hydrogen molecule by the second harmonics of Nd:YAG [532 nm] and Nd:YLF [527 nm] lasers, which has been most extensively characterized (Yang *et al* 1991). The ionization potential of H_2 for the vibrationless ground state is 15.425 eV, requiring absorption of at least seven green photons for ionization. Figure 7 shows the photoelectron spectra (PES) at different laser intensities for 532 nm and 527 nm excitation. The spectra show clearly resolved peaks below 1.3 eV which are assignable to different vibrational quanta of the ground ionic state following seven-photon ionization. Furthermore, as the intensity is increased, behaviours well known from atomic strong-field ionization studies become evident. The first two (7+1, 7+2 absorption) ATI peaks above 1.3 eV are visible, along with strong-field 'channel closure' of low-energy electrons which is caused by the increasing binding energy of the H_2 molecule in the field and is proportional to the ponderomotive potential. However, the most striking feature in figure 7 from the standpoint of our discussion is the strong intensity dependence of the ion vibrational distribution. For example at low intensity, figure 7(c) exhibits well resolved $v^+ = 0$–3 vibrational bands with an intensity distribution that is indicative of Franck–Condon factors from a direct *non-resonant* seven-photon ionization between the $H_2\,{}^1\Sigma_g^+$ and the $H_2^+\,{}^2\Sigma_g^+$ ground states. As the laser intensity is increased, the PES is dominated by the $v^+ = 0$ vibration which signifies the influence of a Rydberg intermediate resonance. In fact, PES studies using H_2, D_2 and HD at two slightly different wavelengths (532 and 527 nm) have resulted in the unambiguous assignment of the $H_2 J\,{}^1\Delta_g(v = 0)$ intermediate state as dominating the ionization dynamics, with some contribution from the $H_2 I\,{}^1\Pi_g$ state at higher intensities. In the dissociation experiments this translates into H_2^+ target molecules with non-stationary vibrational distributions which are spatially distributed throughout the interaction volume. However, as we shall see in section 4.1, the PES studies discussed

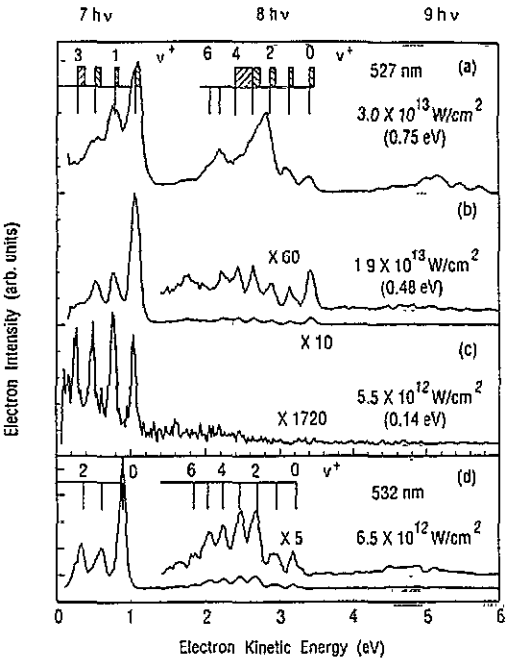

Figure 7. Photoelectron spectrum of H_2 molecule taken at different laser intensities with 527 and 532 nm radiations. The spectra are normalized for gas density and number of laser shots. The tick marks indicate the unperturbed vibrational levels of the H_2^+ ground state. The numbers in parentheses are the ponderomotive energies at each intensity. From Yang *et al* (1991).

above provide enough detailed information that the initial conditions for dissociation of the molecular ion are adequately defined.

Less is known about the initial H_2^+ vibrational distribution at the other wavelengths at which strong-field dissociation has been studied. Investigations at 1 μm are hampered by the limited PES resolution coupled with spectral congestion caused by highly non-linear ionization (14-photon minimum). Figure 8 shows the PES of H_2^+ at two different 1.06 μm intensities (Yang and DiMauro 1993). The photoelectron distribution at low intensity, figure 8(a), can be characterized as a broad distribution peaked at 5 eV and a maximum kinetic energy of 15 eV. However, the spectrum still shows resolvable structure which is assignable to the first four vibrational levels of the H_2^+ ground state. As the laser intensity is increased in figure 8(b), the photoelectron spectrum becomes structureless and shifted towards higher kinetic energy, and consequently a less effective diagnostic tool. Recent studies (Zavriyev *et al* 1993) using 100 fs, 0.8 μm excitation from a titanium sapphire laser are hampered by the fact that the pulses are in the short-pulse limit. At very low intensities, short-pulse Rydberg intermediate resonances are observed (Sheehy and DiMauro 1994) in the PES but with no vibrational information for the reason discussed above. Efforts at better defining stationary initial conditions of the molecular ion are underway (Wunderlich and Hansch 1994, Sheehy and DiMauro 1994) but are much too preliminary for this review.

4. Fragmentation mechanisms

We now present a summary of experimental and theoretical results obtained by various groups over the past few years. Calculations have been performed for a wide range of initial vibrational levels ($v_0 = 0$–14) and for several wavelengths used in recent experiments (248 nm, 330 nm, the first three harmonics of a 1064 nm Nd:YAG laser, 769 nm and 780 nm). The last two wavelengths are in the domain of a subpicosecond titanium sapphire laser.

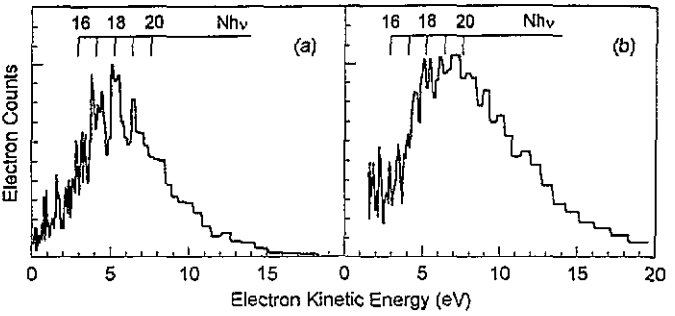

Figure 8. Photoelectron spectrum of H_2 molecule obtained at different 1.06 μm intensities: (a) 2.3×10^{12} W cm^{-2}; (b) 4.1×10^{12} W cm^{-2}. The tick marks indicate the number of absorbed photons above the H_2 ground state. From Yang and DiMauro (1993).

The experimental intensities ranged over 10^{12}–10^{15} W cm^{-2} and the pulse durations from 10 ns to 100 fs, with better interface between theory and experiment offered by the short-pulse results. In a very schematic way the various strong-field physical phenomena can be categorized as low, intermediate and high vibrational state effects. The exact demarkation between the categories depends principally on the frequency of the laser and can be roughly predicted by examining the position of the diabatic curve crossings of the field-dressed potential curves. However, as stated in the introduction, a better physical insight into the various fragmentation processes is often provided by simple examination of the adiabatic dressed curves, as illustrated in figure 9 for 532 nm excitation.

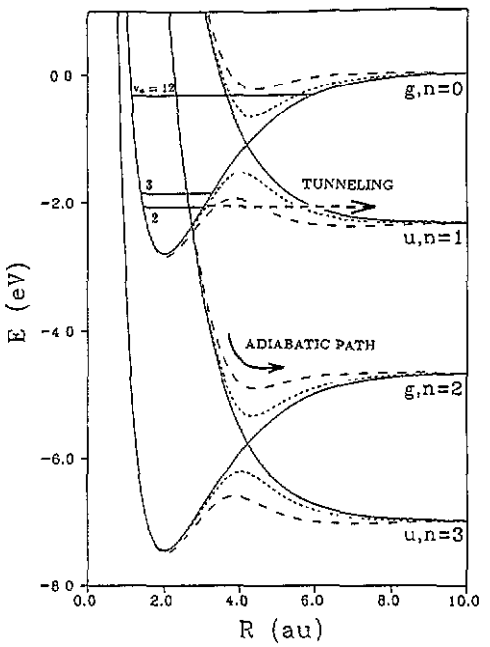

Figure 9. Dressed potential curves for 532 nm in the region of the avoided crossing points which dominate the dissociation mechanisms. The adiabatic curves result from diagonalizing the length-gauge interaction for the intensities 10^{13} W cm^{-2} (----), 4×10^{13} W cm^{-2} (– – –). The vibrational levels indicated correspond to the *diabatic* dressed ground state. They illustrate the alternative decay mechanisms ($v_0 = 2$, above threshold dissociation; $v_0 = 3$, bond-softening; $v_0 = 12$, population trapping).

4.1. Above-threshold dissociation versus bond-softening

The low vibrational states result in above-threshold dissociation (ATD) (Giusti-Suzor *et al* 1990) which is analogous to the well studied effect in atomic photoionization called

above-threshold ionization (Agostini *et al* 1979). From a simple energetic standpoint, ATD corresponds to the absorption of an excess number of photons beyond the minimum needed to break a chemical bond. This is illustrated in figure 9 by considering the $v_0 = 2$ level for the g, $n = 0$ potential. The total energy of this level, and all higher levels, lie above the u, $n = 1$ asymptote and, consequently, can photodissociate by absorbing a single 532 nm photon. However, as indicated by the horizontal broken line in figure 9, this would require extensive tunnelling through a classically forbidden barrier which will be highly improbable at the given intensity. An alternative and more probable path for the $v_0 = 2$ fragmentation is ATD which exists due to the favourable proximity with the u, $n = 3$ crossing (three-photon absorption). Clearly, the balance between ATD and one-photon absorption will depend strongly on the initial vibrational state, laser frequency and intensity. Thus, it is conceptionally useful to think of the strong-field photodissociation as a kind of *laser-induced predissociation* with the *coupling strength at the disposal of the experimentalist.* For instance, let us consider the fate of the $v_0 = 2$ level following three-photon absorption or passage on the u, $n = 3$ curve. Depending upon the intensity, the evolving wavepacket near the avoided crossing at $R = 4.2$ au can either make a diabatic passage and continue on the u, $n = 3$ curve or an adiabatic transition to the u, $n = 2$ curve. However, for an intensity high enough that the crossing at $R = 4.2$ au is strongly avoided, the photofragments will almost exclusively follow the adiabatic path shown in figure 9 and achieve the kinetic energy dictated by the g, $n = 2$ asymptote. The overall process can be seen as fourth order with an initial three-photon absorption near $R = 2$ au followed by a one-photon stimulated emission near $R = 4.2$ au, thus resulting in a net two-photon absorption in terms of asymptotic fragment energy. The corresponding proton kinetic energy distribution (figure 10(a)) is indeed dominated by a two-photon peak near 1.2 eV, with very weak one-photon and three-photon additional peaks on each energy side, separated from the main one by 1.16 eV $= \hbar\omega/2$, the energy of one photon equally shared between the ion and neutral fragments. This result illustrates our introductory remark that the radiative field plays an active role throughout the evolution of the fragmentation process.

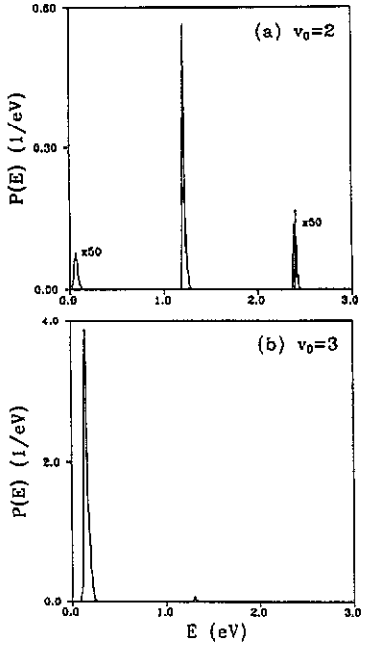

Figure 10. Calculated proton energy distributions in the dissociation process of H_2^+ ground state for initial vibrational levels (a) $v_0 = 2$, (b) $v_0 = 3$. The laser parameters are $\lambda = 532$ nm, $I = 5 \times 10^{13}$ W cm^{-2} and pulse half-duration $T_p = 150$ fs. The successive peaks are separated by half a photon energy (1.16 eV), the second and third peaks corresponding to ATD. Note the contrasted mechanisms for $v_0 = 2$ (ATD) and $v_0 = 3$ (BS) dissociation.

As the initial vibrational state is increased, for a prescribed intensity, we eventually come to some intermediate value, such as $v_0 = 3$ in figure 9, which sits above the adiabatic potential barrier. Consequently, the molecule can undergo rapid over-the-barrier one-photon dissociation as shown in the energy distribution of figure 10(b), where the first peak now largely prevails over the very small two-photon ATD peak. This process which results in a profound local deformation of the molecular potential induced by the strong radiative interaction has been appropriately termed 'bond-softening' by Bucksbaum *et al* (1990). It should be apparent from the adiabatic curves that as the laser intensity increases the barrier will move down to lower vibrational levels. In fact, for sufficiently high intensities even the $v_0 = 2$ level will be subjected to bond-softening and the ATD mechanism will be effectively quenched.

More generally, higher intensity favours more adiabatic behaviour of the fragmentation process. A convincing illustration has been given by Jolicard and Atabek (1992) for 330 nm. Figure 11 shows the dissociation dynamics over two orders of magnitude in intensity. At low intensity the proton spectrum is dominated by three-photon ATD, although weak, but at the highest intensity the spectrum evolves almost exclusively into slow protons resulting from one-photon bond-softening. For intermediate intensity values (approximately 5×10^{13} W cm^{-2}) the dominant feature corresponds to the net two-photon dissociation described above.

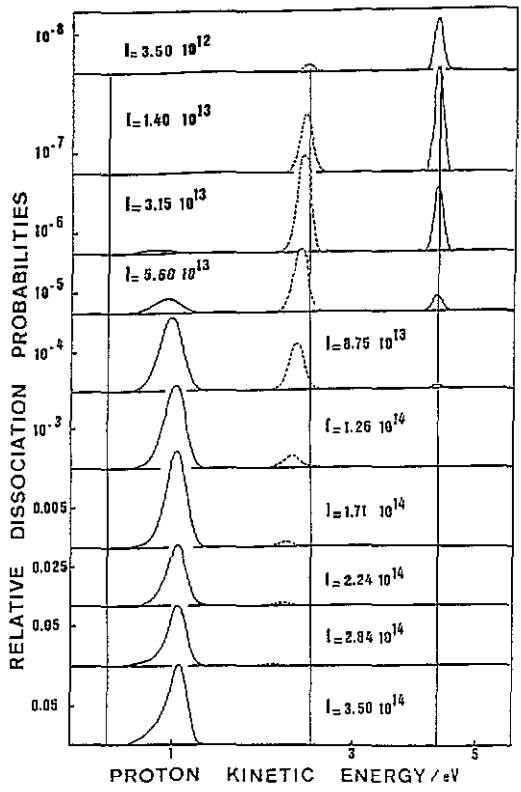

Figure 11. Calculated proton energy spectrum for dissociation of the $v_0 = 0$ level of H_2^+ ground state with $\lambda = 330$ nm, pulse half-duration $T_p = 20$ fs, and various laser intensities as indicated in the figure (in W cm^{-2}). From Jolicard and Atabek (1992).

The experimental observation of these competing fragmentation processes is now well established, in spite of the difficulties associated with ion state preparation (see section 3.2). The first experimental demonstration of both these effects was reported by Bucksbaum *et*

al (1990, see also Zavryiev *et al* 1990). Figure 12 is a proton kinetic energy spectrum resulting from excitation with 100 ps, 532 nm pulses at 5×10^{13} and 10^{14} W cm^{-2}. The spectrum shows peaks which were identified as the one-, two- and three-photon dissociation of the hydrogen molecular ion, spaced by nearly half a photon energy as expected. The photodissociation in this experiment is dominated by the bond-softening mechanism. Figure 12 also shows the angular distribution of the protons, strongly peaked along the polarization direction. Historically, in an earlier experiment studying the Coulomb explosion at 600 and 248 nm, Colding *et al* (1988) did observe shoulders on the high-energy side of the proton peaks in the time-of-flight spectrum, with the appropriate half photon spacing. These peaks were not associated with ATD at that time but, in retrospect, their systematics seem beyond coincidence (Codling and Frasinski 1993).

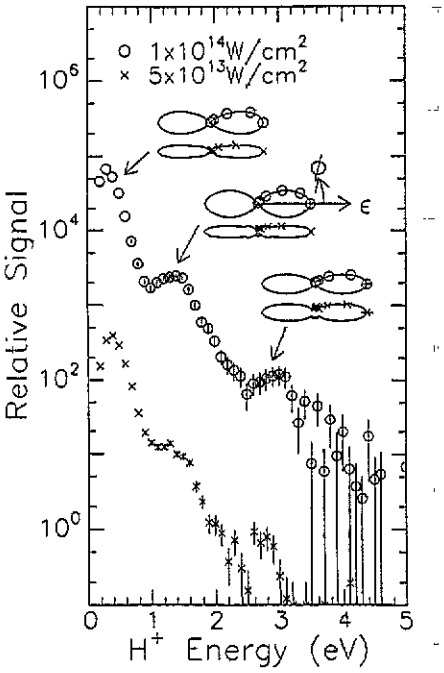

Figure 12. Proton kinetic energy and angular distributions measured at 532 nm, for two intensities (50 and 100 TW cm^{-2}). The peaks at 1.5 and 3 eV correspond to the ATD channels, and the lowest one corresponds to bond-softening. From Bucksbaum *et al* (1990).

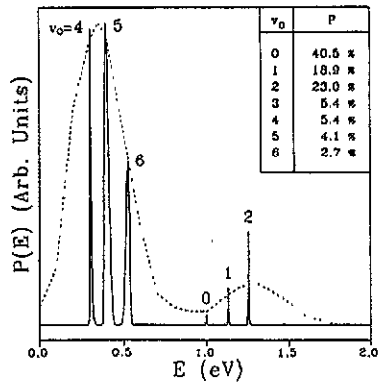

Figure 13. Comparison between calculated (full curve) and experimental (broken curve) proton spectra for 532 nm dissociation. The calculations are done for the intensity 1.45×10^{13} W cm^{-2} (see text) with the initial vibrational distribution given in the inset, derived from the experimental PES (figure 7(d)).

Figure 13 is a comparison between experiment and theory for H_2^+ photodissociation with 532 nm excitation. The experimental proton energy distribution (Yang *et al* 1991) is shown as the dotted curve for the bond-softening and two-photon peak at an intensity of $9.7(\pm 4.8)10^{12}$ W cm^{-2}. The full curve is calculated using the initial vibrational population derived from the PES and an intensity of 1.45 10^{13} W cm^{-2} which is within one standard deviation of the experimental value. There is no spatial or temporal averaging in the theoretical curve. The agreement between the two curves is very good, although the theory seems to underestimate the contribution of $v_0 > 2$ for ATD. From this plot it is clear that

the separation between the one- and two-photon peaks is less than half a photon energy since they originate from different initial vibrational levels. Furthermore, not all of the two-photon peak can be characterized as ATD, since for $v_0 > 2$ the two-photon process is the lowest allowed order.

An experiment by Yang *et al* (1991) studied the intensity-dependent dynamics of these processes for hydrogen and deuterium molecular ions using 532 and 527 nm excitation. Photoelectron spectra (figure 7) were recorded in conjunction with the fragment spectra to characterize the initial vibrational state of the ions. Figure 14 is a compilation of the branching ratios R_{ab} for the various n-photon processes as a function of intensity. The open symbols (triangles, D_2^+ and circles, H_2^+) are the ratios of total ATD to bond-softening and the full symbols are the ratios R_{32} of three- to two-photon dissociation. Both isotopes show that the amount of high-energy fragments (ATD) increases with higher intensities. This contradicts the theoretical findings for a given vibrational level (see figure 11), but is easily rationalized if the high v populations in figure 13, which would decay mostly in the one-photon channel, are sensitive to intensity or saturated. On the other hand, the ratio R_{32} decreases with increasing intensity, as expected. This shows the propensity for adiabatic passage at $R \approx 4.2$ au due to the widening gap of the avoided crossing (figure 9). Furthermore, at the lowest intensity $R_{32}(H) > R_{32}(D)$, because the D_2^+ molecules with lower vibrational frequency branch more efficiently through the two-photon adiabatic path than H_2^+. In other words, lower vibrational frequency implies more adiabatic motion when passing the avoided crossing.

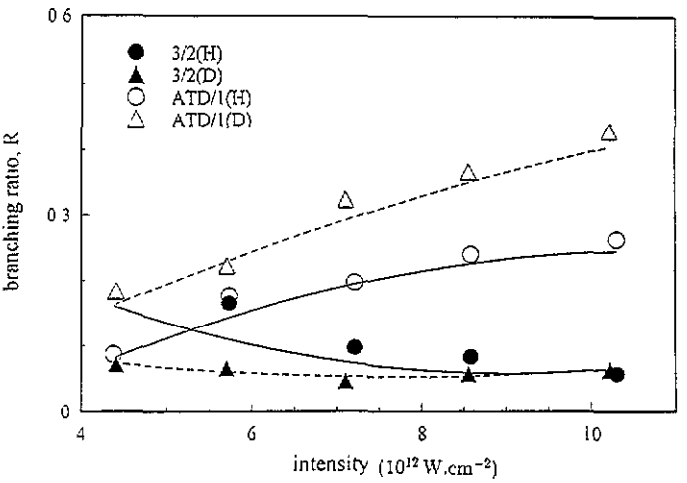

Figure 14. Plot of the ATD branching ratios R_{ab} as a function of 532 nm intensity, for H_2^+ and D_2^+. The open symbols are the branching ratio of the total ATD against bond-softening and the full symbols represent the three- over two-photon dissociation. From Yang and DiMauro (1993).

The wavelength dependence of the photodissociation dynamics can be demonstrated by examining the fragmentation at 1064 nm (Yang and DiMauro 1993). Figure 15(a) is a plot of the time-of-flight spectrum. The peaks labelled a and b correspond to two- and four-photon dissociation, respectively, and are the only peaks observed over the dynamic range of the experiment. Here the ATD ratio (R_{42}) increases with rising intensity, contrarily to the R_{32} ratio at 532 nm. The 1064 nm behaviour is more analogous to the intensity dependence observed in ATI (Agostini *et al* 1979), that is, higher intensity results in higher

energy particles. This strong wavelength dependence, resulting in such different dynamics, is consistent with the dressed-state model shown in figure 15(b). Following absorption of three and five photons, adiabatic passage (implying stimulated emission of one photon) dominates at the avoided crossings $R \approx 5$ au and results in only two- and four-photon fragmentation. Thus, the increase in the R_{42} ratio results from the fact that each proton peak originates from a different order process with the highest one (fifth order) becoming more efficient at higher intensities. The bond-softening plays no role in this experiment because high vibrational states are not populated in the molecular ion (see section 3.2 and figure 8).

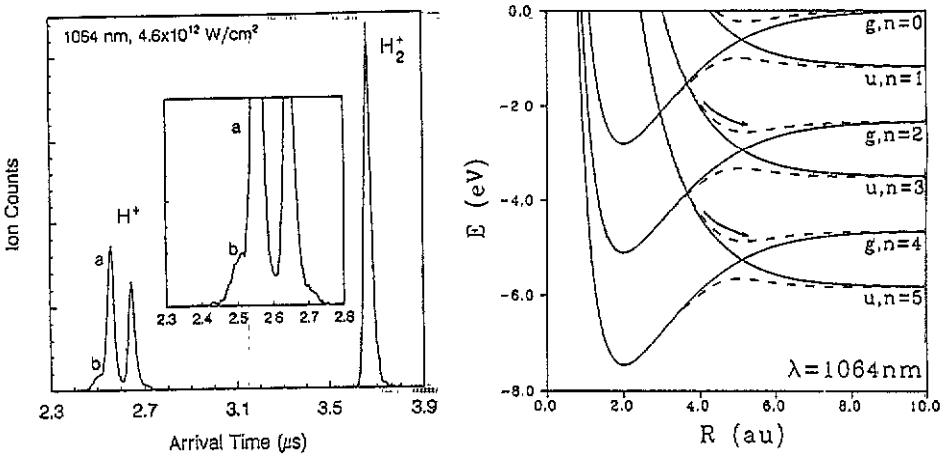

Figure 15. Time-of-flight mass spectrum of H_2 resulting from 1.06 μm excitation at the intensity 4.6×10^{12} W cm^{-2}. The peaks labelled a and b correspond to the forward velocity protons formed via two- and four-photon dissociation of H_2^+ respectively, with an expanded view of the proton distribution. From Yang and DiMauro (1993). The diagram on the right shows the dressed potential curves for $\lambda = 1.06$ μm (——, diabatic; - - - -, adiabatic for the intensity 10^{13} W cm^{-2}). The g, $n = 2$ and g, $n = 4$ dissociations observed mainly follow the adiabatic paths to asymptotic limits.

4.2. Population trapping and molecular stabilization

As we go to initial vibrational levels above $v_0 = 8$ for $\lambda = 532$ nm, which now energetically lie above the crossing of the g, $n = 0$ and u, $n = 1$ curves in figure 9, we discover that the probability of photodissociation suddenly decreases because a portion of the initial vibrational population is 'trapped' in the adiabatic well formed by the avoided crossing. This trapping effect for $\lambda = 532$ nm was calculated to peak at $v_0 = 12$ for the intensity 2.5×10^{13} W cm^{-2} (Giusti-Suzor and Mies 1992, figure 3) and was also found at various other wavelengths (Giusti-Suzor and Mies 1992, Yao and Chu 1992, 1993, Aubanel *et al* 1993a, b). It is related to the light-induced bound states postulated by Fedorov *et al* (1975), Yuan and George (1978) and Bandrauk and Sink (1981) for CW lasers at specific intensities, and recently used by Atabek *et al* (1994) to predict an isotope separation in the D_2^+–H_2^+ system subjected to a CW UV laser. But the population trapping described here appears to occur even when short-pulsed lasers with rapidly varying laser intensity are used. Of course the effect still depends on the peak intensity which determines the adiabaticity. If

the intensity is too low the adiabatic curve will not support the trapped population. If the intensity is too strong the adiabatic well will be destroyed and the 'trapped' population will escape via the g, $n = 0$ asymptote and yield photofragments with an unusually low kinetic energy.

The experimental evidence for trapping is not very conclusive, but Zavriyev *et al* (1993) observed some convincing 'signatures' of this effect using 150 fs, 769 nm excitation. Their results are in qualitative agreement with the proton spectra presented in figure 16, from presently unpublished data (Sheehy and DiMauro 1994) at 780 nm. We shall join those authors in their speculation that the higher energy peak above 1 eV is not due to direct photodissociation of H_2^+ but rather originates from the photoionization of field-dressed vibrationally trapped molecular ions. The kinetic energy of the proton 'measures' the Coulomb repulsion that the residual pair of protons in equation (1*b*) experiences following the photoionization of H_2^+, and the proton kinetic energy $\varepsilon_{H^+} \approx e^2/2R$ represents a mapping of the interatomic coordinate R at the 'moment' of ionization. This is a manifestation of the so-called 'Coulomb explosion' that has been reviewed by Codling and Frasinski (1993).

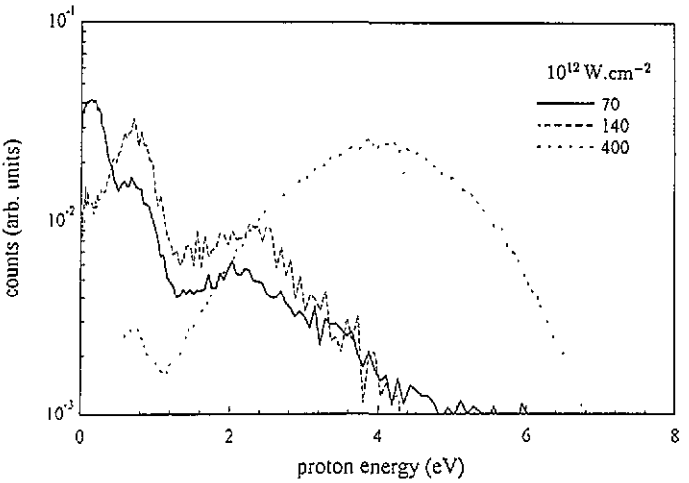

Figure 16. The proton kinetic energy spectrum of H_2 at different 780 nm laser intensities. From Sheehy and DiMauro (1994).

The adiabatic field-dressed curves at this wavelength (figure 17) show that the $v_0 = 12$ level lies above the u, $n = 1$ crossing and will exhibit the same trapping phenomenon as seen at 532 nm. In addition, trapping may occur in other *multiphoton* potential wells, such as the adiabatic well formed between the crossing of the u, $n = 3$ and g, $n = 0$ potential curves. This well will be accessible to lower vibrational states, i.e. $v_0 = 4$ and 5 and has been proposed (Zavriyev *et al* 1993; see also the theoretical study by Yao and Chu 1993) as the source of the trapped population in the experiment. Aubanel *et al* (1993b) have demonstrated the trapping effect for $v_0 = 5$ as a function of peak intensity in their figure 4, for the two-state field-aligned model labelled as $J = 0$. The $v_0 = 5$ results in figure 18 are in excellent agreement with theirs and also demonstrate the absence of trapping for $v_0 = 3$ and the occurrence of trapping for $v_0 = 4$ at a peak intensity near $I = 1.7 \times 10^{14}$ W cm^{-2}.

The trapping effect is seen very clearly in the time evolution of the wavepackets in figure 19 which are produced by a $T_p = 150$ fs pulse. We show both the $v_0 = 12$ state

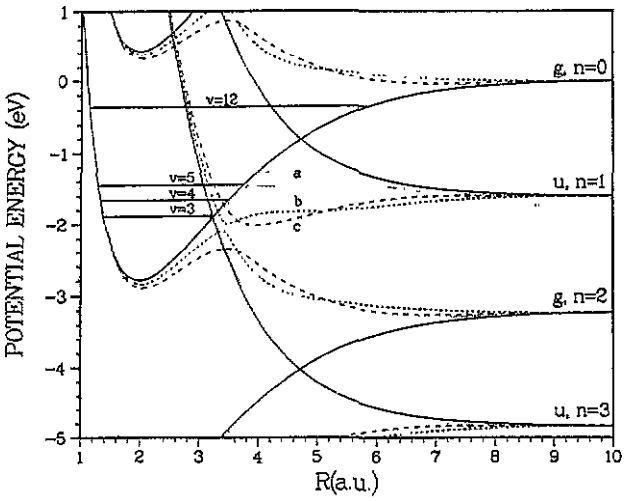

Figure 17. Dressed potential curves for $\lambda = 780$ nm. The full curves are the diabatic curves dressed with 0–3 photons, the others are the adiabatic curves for the three intensities: (a) 5×10^{12}; (b) 5×10^{13}; (c) 10^{14} W cm^{-2}.

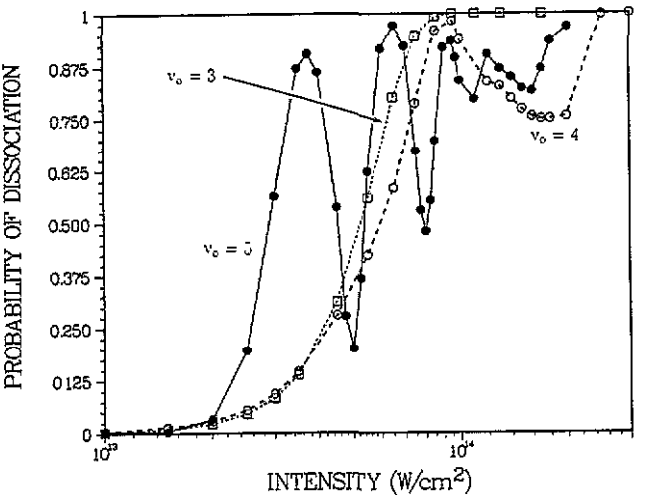

Figure 18. Dissociation probability as a function of 780 nm radiation intensity, for pulse half duration 150 fs and initial vibrational levels $v_0 = 3$ (open squares), $v_0 = 4$ (open circles), $v_0 = 5$ (full circles).

subjected to a peak intensity of $I = 1.5 \times 10^{13}$ W cm^{-2}, which becomes trapped in the $n = 1$ adiabatic well (see Aubanel *et al* 1993b, figure 3), and the $v_0 = 4$ state subjected to a peak intensity of 1.7×10^{14} W cm^{-2}, which becomes trapped in the $n = 3$ adiabatic well. More precisely we plot the sum $|F_u(R)|^2 + |F_g(R)|^2$ of the squared components of the two-channel wavepacket in equation (4), which gives the total probability of finding it located at the internuclear distance R. We only show the packet in the region $R = 0$–10 au where trapping occurs (the portions that extend beyond this region almost invariably lead

to dissociation). What is striking in both cases is that after having dissociated a certain percentage of the molecules in the leading edge of the laser pulse, up to $t \approx 60$ fs for $v_0 = 12$ and $t \approx 100$ fs for $v_0 = 4$, suddenly the field is strong enough to trap the remainder of the molecules in a dressed 'bound state' at 4–7 au where the system becomes immune to further dissociation, *even though the laser has yet to reach its peak power* at $t = 150$ fs. Finally on the trailing edge of the pulse, the field has decreased sufficiently so that the trapping ceases and photodissociation resumes, with a further fraction of the molecules experiencing fragmentation and the rest being redistributed on field-free bound levels close to the initial one.

The bound-state character of the trapped states is evident in figure 19. At the peak intensity the $v_0 = 12$ forms a $v \approx 1$ like vibrational state in the adiabatic $n = 1$ field-dressed potential. The norm of the trapped portion remains at about 73% in this dressed state for about ±40 optical cycles on each side of the peak, out of a total of 117 cycles for the entire pulse. On the other hand the $v_0 = 4$ level becomes trapped in a $v \approx 0$ level formed by the $n = 3$ field-dressed potential and only persists for about ±23 optical cycles with a norm of about 48%.

These calculations were all performed in the 1D approximation with the molecule perfectly aligned in the field. Aubanel *et al* (1993b) have found that including the molecular rotations in a full 3D treatment can partially suppress the trapping effect. We confirm their finding, at least for the rotationally excited $v_0 = 5$ levels which actually lie *above* the $n = 3$ dissociation limit. For example the $(v_0 = 5, N_0 = 5, M_0 = 0)$ level is 90% dissociated in the 3D calculations instead of only 22% for the rotationless $v_0 = 5$ level in the 1D model. However, if we start from an initial $(N_0 = 1, M_0 = 0)$ level the stabilization persists in the full 3D calculations with a *negligible increase in dissociation* from 22% to 23%. Similarly the stabilization is much more robust for the $v_0 = 4$ and the trapping phenomenon is not nearly as sensitive to being suppressed by a full 3D treatment. In any case, in order to interpret the experiments we are relying on the packet being trapped in the adiabatically dressed vibrational states for a significant time *during the peak of the pulse* where we can most expect ionization to occur, and this qualitative feature remains in both the 1D and 3D calculations.

We conclude this section by pointing out some features observed in the theoretical proton kinetic energy distributions when trapping occurs, with speculations about the connection with the experimental observations. The distribution in figure 20(a) is obtained from an asymptotic analysis of the wavepacket in figure 19(b), originating from the $v_0 = 4$ dissociation. It consists of a weak u, $n = 1$ peak near threshold and a more pronounced g, $n = 2$ peak at 0.63 eV. The oscillations observed in this peak are due to quantum interferences between two similar packets of continuum states which originated during the leading and trailing edges of the pulse (see figure 19(b)), i.e. before and after the N_{tr} optical cycles during which trapping occurs, and are thus separated in time by $\Delta_{tr} = 2\pi N_{tr}/\omega$. It is easy to show that this phenomenon gives rise to equally spaced oscillations in the proton kinetic energy spectrum with a separation given by $\delta\varepsilon^+ = \frac{1}{2}\hbar\omega/N_{tr}$ (the factor of 1/2 comes from sharing the kinetic energy between the proton and the neutral fragment), which is consistent with the 0.017 eV uniform spacing observed in figure 20 with a trapping lasting for $N_{tr} \approx 47$ optical cycles. This feature has been found in all theoretical energy distributions involving trapping (Giusti-Suzor and Mies 1992, Yao and Chu 1993) and can be used as a signature that significant trapping effects are occurring in a dissociation event, although they might be difficult to detect experimentally.

There are no higher ATD peaks in the calculated photodissociation spectrum, while fast protons are observed in the experimental results of figure 16. However, if we

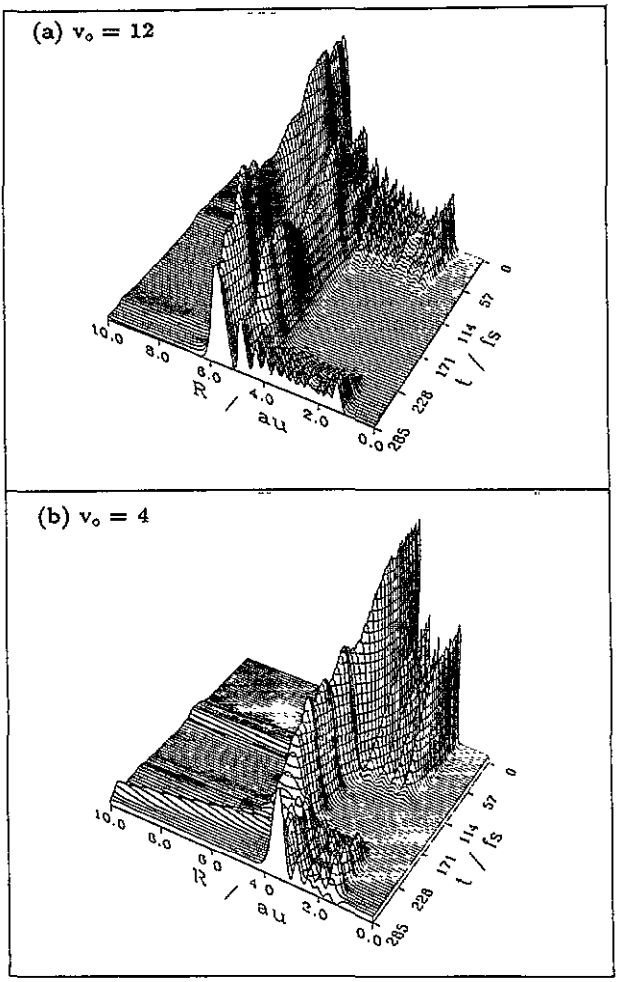

Figure 19. Time evolution of the radial wavepacket during the 300 fs entire pulse duration of a 780 nm laser, for initial vibrational level: (a) $v_0 = 12$, with partial trapping in the upper $n = 4$ adiabatic well of figure 17 ($I = 1.5 \times 10^{13}$ W cm^{-2}); (b) $v_0 = 4$, trapped in the lower $n = 3$ adiabatic well ($I = 1.7 \times 10^{14}$ W cm^{-2}).

assume that the H_2^+-photoionization rate only depends on R and that the probability of experiencing a Coulomb explosion in the vicinity of the peak intensity is proportional to the radial distribution of the molecular wavepacket at the moment of ionization, we obtain the additional broken peak in the proton spectrum shown in figure 20(b). The relative contribution of the Coulomb peak to the calculated photodissociation spectrum is completely arbitrary and the two spectra should only be compared with regard to their energy distributions. In this respect, the theoretical distribution bears a very good resemblance to the $1.5–2 \times 10^{14}$ W cm^{-2} spectra in figure 16. Furthermore, the general shift of the 'Coulomb peak' towards higher energy with increasing intensity in the observed spectra is consistent with our expectation from the ionization calculations presented in section 2.5: the ionization probabilities shown in figure 6 favour larger R and therefore smaller Coulomb repulsion for the exploding ions at weaker intensity.

Certainly most of the general trends in the experimental data are consistent with this

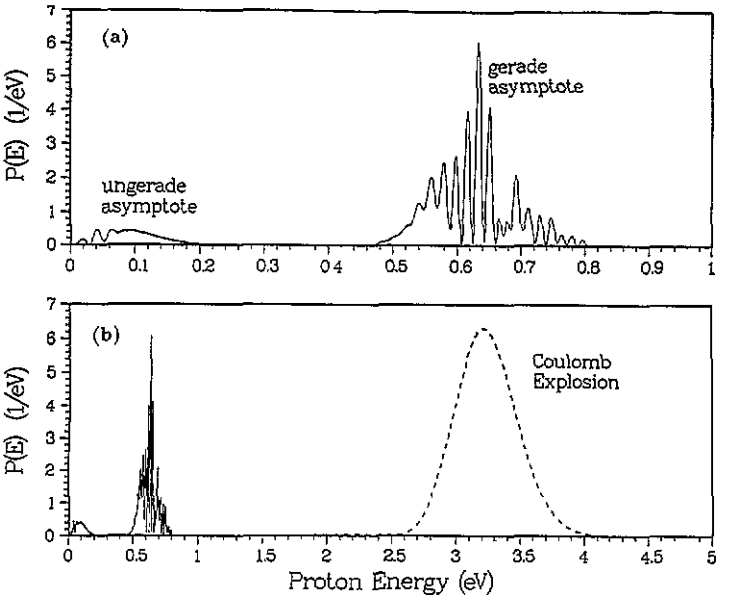

Figure 20. Calculated proton energy distribution on two different energy scales for 780 nm dissociation of initial $v_0 = 4$ level, laser intensity 1.7×10^{14} W cm^{-2} and pulse half duration 150 fs.

simple trapping model + Coulomb explosion, as first proposed by Zavriyev *et al* (1993), and we find the agreement with the calculations very convincing. Two questions remain: how can we justify the important role of the $v_0 = 3$–5 states; and how can this model explain the ubiquitous appearance of about 0.2 eV oscillations in the proton energy spectra?

First, we must assume the initial ionization produces an ensemble of vibrational states with a reasonable population in $v_0 \geqslant 3$. Both the ionization and dissociation rates are very small for H_2^+ in $v_0 = 0, 1, 2$ at these intensities, so they simply do not contribute significantly to the spectra. Even though the $v_0 = 3$ state is completely dissociated at high intensities, we have seen in figure 5 that portions of the packet are trapped in the leading edge of the pulse, thus avoiding the 'Lambropoulos curse' (Lambropoulos 1985) and surviving to experience the peak intensity.

Examining the wavepackets for the trapped $v_0 = 5$ state at various peak intensities, we have found that trappings around 10^{14} W cm^{-2} (see figure 18) involve *coherent* admixtures of $v = 0, 1$ and 2 levels in the $n = 3$ adiabatic well. Ionization thus occurs over a more extended R region than for the $v_0 = 4$ state which is trapped in the $v \approx 0$ adiabatic state (see figure 19(b)), and this would broaden the Coulomb peak simulated in figure 20(b). In addition the periodic motion of the coherent vibrational wavepacket might help explain the small, but reproducible oscillations in the observed spectrum. On the other hand, Zavriyev *et al* (1993) suggest that the initial ionization of the neutral H_2 molecule in such a short pulse might produce a coherent superposition of initial v_0 levels with a recursion time that can also contribute to the oscillations. This proposal is attractive, but has yet to be put into rigorous time-dependent calculations.

4.3. Two-colour coherent control of intense field dissociation

The last process we wish to advertise in this review is two-colour photodissociation

performed by superposing two harmonics of the same radiation (typically the fundamental together with the second or third harmonic), assuming a constant phase-shift between them (phase-locked regime). This device is expected to provide a better control of the dissociation dynamics than just varying the laser wavelength and intensity as was done in the one-colour experiments. The second frequency adds alternative pathways towards each fragmentation limit, thus generating interference effects very sensitive to phase variations (Shapiro *et al* 1988). In addition, an interesting asymmetric dissociation of H_2^+ and HD^+ is predicted in the case of the second harmonic. Encouraged by similar theoretical (Schafer and Kulander 1992) and experimental studies on atomic two-colour photoionization (Muller *et al* 1990, Yin *et al* 1992, Schumacher *et al* 1994), we have good expectations that one can 'coherently' control the alternative fragmentation mechanisms described above. Preliminary experiments for H_2^+ and HD^+ are very promising (Sheehy and DiMauro 1994).

The dissociation is induced here by a superposition of two fields given by

$$E(t) = f(t)[E_f \cos(\omega t) + E_h \cos(n_h \omega t + \varphi)]\hat{e} \tag{19}$$

where E_f and E_h are the maximum field amplitudes for the fundamental and harmonic radiations respectively, φ the 'locked' phase difference between them, and $n_h = 2$ or 3 for the second or third harmonic. The Gaussian-like pulse shape $f(t)$ and polarization vector $\hat{e}$ are assumed to be identical for both radiations. Exactly the same time-dependent calculations as for the one-colour case (see section 2.3) can be performed with this two-colour field.

The first feature to be noted (Charron *et al* 1993) is the large change in the total dissociation probability when two harmonics are superimposed compared to the probabilities obtained with each separate harmonic. The dissociation efficiency may increase or decrease by more than two orders of magnitude, mainly due to constructive or destructive interference between the different pathways. This effect strongly depends on the intensity of each harmonic and on their relative phases, which also acts on the differential and partial rates.

Varying the phase between the two harmonics has been found to dramatically change the kinetic energy distribution of the photofragments, due to complex interference between the absorption and stimulated emission of the two types of photon. This is demonstrated in figure 21 for 780 nm radiation and its 260 nm third harmonic. Dissociation occurs almost exclusively through ATD for the phase difference $\varphi = 0$, but is instead dominated by the bond-softening (one photon) process for $\varphi = \pi$. This behaviour has been checked to be very 'robust' with respect to uncertainties in the intensity or phase values, and it should allow an appreciable control of the fragmentation dynamics.

Finally, a phase-controllable asymmetry of proton ejection can be obtained when one harmonic is an even multiple of the other one, e.g. $(\omega + 2\omega)$. This can be understood from the angular distribution formula (18) derived in section 2.4 for the 3D calculations: both gerade and ungerade amplitudes contribute in this case to the same energy peak, resulting in a non-vanishing interference term $C_g^* C_u$ which changes sign between forward $(\theta = 0)$ and backward $(\theta = \pi)$ proton ejection. An example is shown in figure 22 for the 780 nm radiation and its 390 nm second harmonic, with two different values of the phase φ (Charron *et al* 1994a). The intensities of both harmonics were kept low enough (4×10^{13} and 4×10^{12} W cm^{-2} respectively) to prevent too much ionization of the neutral fragment on its way to the detector, which would attenuate the asymmetry.

Although this review is restricted to the H_2^+ results, it is worth mentioning that similar calculations have now been performed for the HD^+ isotope (Charron *et al* 1994b). Adequate modifications in the molecular Hamiltonian and radiative couplings include the effect of the permanent dipole associated with the separation of the centre-of-charge and the centre-of-mass in this heteronuclear system. This induces rovibrational transitions *within* each of the

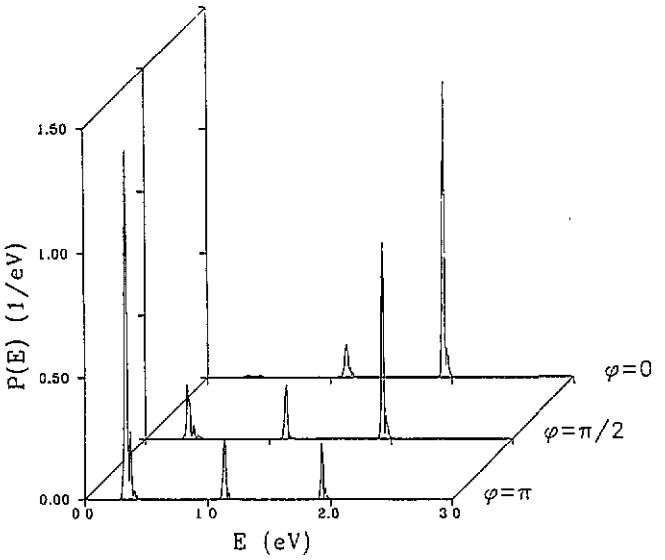

Figure 21. Proton kinetic energy distribution for different phases ($\varphi = 0, \pi/2, \pi$) of the third harmonic (260 nm, $I_h = 5 \times 10^{12}$ W cm^{-2}) with respect to the fundamental radiation (780 nm, $I_f = 10^{14}$ W cm^{-2}). The pulse half duration is 150 fs and the initial vibrational level is $v_0 = 1$. From Charron *et al* (1993).

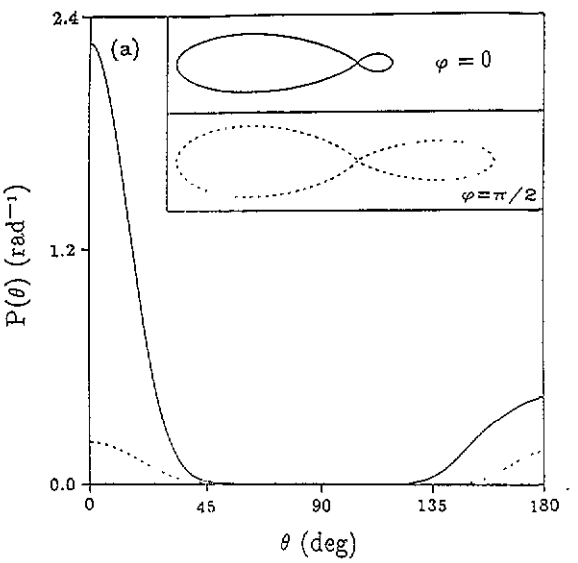

Figure 22. Proton angular distribution obtained from a 3D calculation for two-colour dissociation of initial ($v_0 = 3, N_0 = 1, M_0 = 0$), with 780 nm fundamental ($I_f = 10^{14}$ W cm^{-2}) and 390 nm second harmonic ($I_h = 5 \times 10^{12}$ W cm^{-2}), phase-shifted by $\varphi = 0$ (full curve) and $\varphi = \pi/2$ (broken curve). The pulse half duration is 150 fs. The inset shows the contour plots with respect to the laser polarization axis ($\theta = 0$). From Charron *et al* (1994a).

ground and excited states. In addition the asymptotic limits $H^+ + D(1s)$ and $H(1s) + D^+$ are separated by 29.8 cm^{-1}. Together these effects allow substantial control over the spatial separation of the H^+ and D^+ photofragments to be achieved in the long wavelength limit.

5. Summary and conclusions

The strong-field studies outlined throughout this review exemplify the critical role of the laser field in altering the final outcome of a photodissociation process. The recipe for achieving control over a desired process has at its disposal all the field parameters, i.e. intensity, frequency, phase. The chemist's dream will not be realized until control of a

chemical reaction is fulfilled, but the studies discussed in this review are certainly providing a foundation on which to build. From the standpoint of the hydrogen molecule the future looks bright, the theoretical methods have advanced to the point of achieving good agreement with the experiments and predict that finer control is possible via two-colour phase locking. Future studies exploring the ramifications of temporal shaping or encoding frequency information on light pulses could result in additional flexibility. Also the simultaneous inclusion of further ionization will be beneficial in developing a full understanding of the photophysics of H_2^+.

For experimentalists, the challenge of producing a clean source of hydrogen molecular ions still remains. This is especially imperative as experiments evolve towards sub-picosecond pulse duration where techniques such as PES become less effective. Concomitantly, this short-pulse regime introduces a theoretical challenge since we may no longer be allowed to treat the ionization of H_2 and subsequent dissociation of H_2^+ as a sequence of events with the H_2 ionization simply offering a prescribed distribution of initial *stationary* H_2^+ rovibrational states. Certainly, as implied by Zavriyev *et al* (1993), as the experimental pulse times approach the vibrational period in H_2 and H_2^+ molecules we must allow for the formation of a *coherent* H_2^+ vibrational wavepacket from a simultaneous treatment of H_2 ionization.

Acknowledgments

Two of us (AGS and FHM) thank NATO for partial support from a grant for International Collaborative Research. We are grateful to Harm Geert Muller for supplying us with the unpublished data that we used for the comparisons in figure 3. These represent an elaboration of the results presented in his 1992 paper, and have been decisive for further treatment of H_2^+ dynamics in strong fields. The work carried out at Brookhaven National Laboratory was under contract No. DE-AC02-76CH00016 with the US Department of Energy and supported by its Division of Chemical Sciences, Office of Basic Energy Sciences. Some of the computer facilities were provided by IDRIS of CNRS.

References

Agostini P, Fabre F, Mainfray G, Petite G and Rahman N K 1979 *Phys. Rev. Lett.* **42** 1127
Allendorf S W and Szöke A 1991 *Phys. Rev.* A **44** 518
Atabek A, Chrysos M and Lefebvre R 1994 *Phys. Rev.* A **49** R8
Aubanel E E, Gauthier J M and Bandrauk A D 1993a *Phys. Rev.* A **48** 2145
Aubanel E E, Conjusteau A and Bandrauk A D 1993b *Phys. Rev.* A **48** R4011
Bandrauk A D and Sink M L 1978 *Chem. Phys. Lett.* **57** 569
—— 1981 *J. Chem. Phys.* **74** 1110
Bandrauk A D, Aubanel E and Gauthier J M 1993 *Molecules in Laser Fields* ed A D Bandrauk (New York: Dekker) p 109, and references therein
Bates D R 1951 *J. Chem. Phys.* **19** 1122
Bucksbaum P H, Zavriyev A, Muller H G and Schumacher D W 1990 *Phys. Rev. Lett.* **64** 1883
Charron E, Giusti-Suzor A and Mies F H 1993 *Phys. Rev. Lett.* **71** 682
—— 1994a *Phys. Rev.* A **49** R641
—— 1994b submitted
Chelkowski S, Zuo T and Bandrauk A D 1992 *Phys. Rev.* A **46** R5342
—— 1993 *Phys. Rev.* A **48** 3837
Chrysos M, Atabek O and Lefebvre R 1993 *Phys. Rev.* A **48** 3845, 3855
Chu S-I 1981 *J. Chem. Phys.* **75** 2215

Chu S-I 1991 *J. Chem. Phys.* **94** 7901
Codling K and Frasinski L J 1993 *J. Phys. B: At. Mol. Opt. Phys.* **26** 783
Codling K, Frasinski L J and Hatherly P A 1988 *J. Phys. B: At. Mol. Opt. Phys.* **2** L433
Cornaggia C, Normand D, Morellec J, Mainfray G and Manus C 1986 *Phys. Rev.* A **34** 207
Fedorov M V, Kudrevatova O V, Makarov V P and Samokhin A A 1975 *Opt. Commun.* **13** 299
Feit M J, Fleck J A and Steiger A 1982 *J. Comput. Phys.* **47** 412
Freeman R R and Bucksbaum P H 1991 *J. Phys. B: At. Mol. Opt. Phys.* **24** 325
Freeman R R, Bucksbaum P H and McIlrath T J 1988 *IEEE J. Quant. Electron.* **24** 1462
Gavrila M (ed) 1992 *Adv. At. Mol. Opt. Phys.* Suppl. 1
Gibson G N, Freeman R R and McIlrath T J 1991 *Phys. Rev. Lett.* **67** 1230
Giusti-Suzor A, He X, Atabek O and Mies F H 1990 *Phys. Rev. Lett.* **64** 515
Giusti-Suzor A and Mies F H 1992 *Phys. Rev. Lett.* **68** 3869
He X, Atabek O and Giusti-Suzor A 1988 *Phys. Rev.* A **38** 5586
—— 1990 *Phys. Rev.* A **42** 1585
Heather R W 1991 *Comput Phys. Commun.* **63** 446
Heather R W and Mies F H 1991 *Phys. Rev.* A **44** 7560
Helm H, Dyer M J and Bissantz H 1991 *Phys. Rev. Lett.* **67** 1234
Jolicard G and Atabek O 1992 *Phys. Rev.* A **46** 5845
Keller A 1994 *Phys. Rev.* A submitted
Kroll N M and Watson K M 1976 *Phys. Rev.* A **13** 1018
Lambropoulos P 1985 *Phys. Rev. Lett.* **55** 2141
Lau A M F 1977 *Phys. Rev.* A **16** 1535
McCann J F and Bandrauk A D 1992 *J. Chem. Phys.* **96** 903
Mies F H and Giusti-Suzor A 1991 *Phys. Rev.* A **44** 7547
Mies F H, Giusti-Suzor A, Kulander K C and Schafer K J 1993 *Super Intense Laser–Atom Interactions (NATO ASI Series B 316)* ed B Piraux, A L'Hullier and K Rzazewski (New York: Plenum) pp 329–40
Muller H G 1992 *Coherence Phenomena in Atoms and Molecules in Laser Fields (NATO ASI Series B 287)* ed A D Bandrauk and S C Wallace (New York: Plenum) p 89
Muller H G, Bucksbaum P H, Schumacher D W and Zavriyev A 1990 *J. Phys. B: At. Mol. Opt. Phys.* **23** 2761
Normand D, Cornaggia C and Morellec J 1986 *J. Phys. B: At. Mol. Phys.* **19** 2881
Normand D, Lompré L A, Cornaggia C 1992 *J. Phys. B: At. Mol. Opt. Phys.* **25** L497
Schafer K J and Kulander K C 1992 *Phys. Rev.* A **45** 8026
Schumacher D W, Weihe F, Muller H G and Bucksbaum P H 1994 *Phys. Rev. Lett.* **73** 1344
Shapiro M, Hepburn J W and Brumer P 1988 *Chem. Phys. Lett.* **149** 451
Sheehy B and DiMauro L F 1994 unpublished
Shirley J H 1965 *Phys. Rev.* B **138** 979
Singer J, Freed K F and Band Y B 1983 *J. Chem. Phys.* **79** 6060
—— 1984 *J. Chem. Phys.* **80** 3064
Strickland D T, Beaudoin Y, Dietrich P and Corkum P B 1992 *Phys. Rev. Lett.* **68** 2755
Verschuur J W J, Noordam L D and van Linden van den Heuvell H B 1989 *Bull. R. Soc. Sci.* **58** 293
Wunderlich C and Hansch T 1994 private communication
Yang B and DiMauro L F 1993 *Laser Phys.* **3** 398
Yang B, Saeed M, DiMauro L F, Zavriyev A and Bucksbaum P H 1991 *Phys. Rev.* A **44** R1458
Yao G and Chu S-I 1992 *Chem. Phys. Lett.* **197** 413
—— 1993 *Phys. Rev.* A **48** 485
Yin Y Y, Chen C, Elliott D S 1992 *Phys. Rev. Lett.* **69** 2353
Yuan M and George T F 1978 *J. Chem. Phys.* **68** 3040
Zavriyev A, Bucksbaum P H, Muller H G and Schumacher D W 1990 *Phys. Rev.* A **42** 5500
Zavriyev A, Bucksbaum P H, Squier J and Saline F 1993 *Phys. Rev. Lett.* **70** 1077